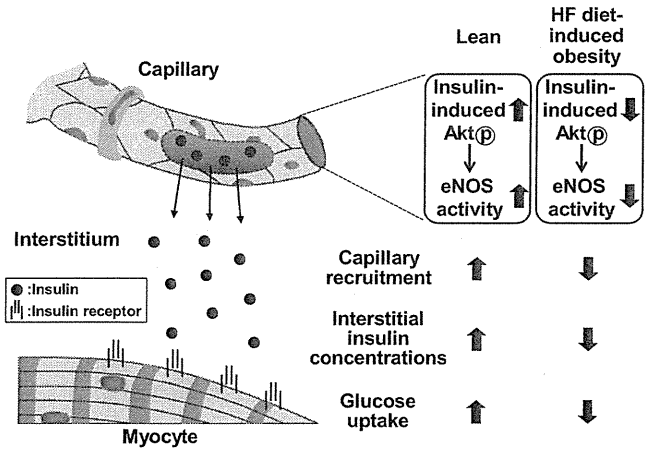

Figure 6. Impaired Insulin Signaling in the Endothelial Cells Reduces Insulin-Induced Glucose Uptake by the Skeletal Muscle in Obese Subjects

In lean subjects, the insulin-mediated Akt and eNOS activations are induced optimally in the endothelial cells after feeding, resulting in insulin-induced capillary recruitment, increase of interstitial insulin concentrations, and increase of the glucose uptake by the skeletal muscle. By contrast, since the insulin-mediated Akt and eNOS activations are inadequate in the endothelial cells of obese subjects after feeding, the insulin-induced capillary recruitment, increase or interstitial insulin concentrations, and increase of glucose uptake by the skeletal muscle are impaired.

Moreover, insulin delivery into the interstitial fluid is known to be delayed in insulin resistance (Sjostrand et al., 2002), as also is the onset of insulin stimulation of glucose uptake (Nolan et al., 1997). In addition, delivery of inulin, a molecule whose molecular weight is similar to that of insulin, to the skeletal muscle was reported to be markedly diminished in diet-induced insulin resistance (Ellmerer et al., 2006). These findings suggest that impairment of insulin delivery, possibly caused by an endothelial insulin signaling defect, may play a critical role in the skeletal muscle insulin resistance seen in obesity.

Why were decreased insulin signaling and decreased glucose uptake in response to insulin observed only in the skeletal muscle of the ETIrs2KO mice and not in their liver? The difference between the types of capillaries in the liver and skeletal muscle may explain these differences in the insulin sensitivity of the two organs. It is thought that the occluded junctions of the endothelial cells of the capillaries in the skeletal muscle may prevent paracellular transport of most macromolecules, including insulin, whereas the fenestrated endothelium of the capillaries in the liver freely permits paracellular passage of macromolecules (Aird, 2007). In fact, more rapid insulin action kinetics have been observed in the liver than in the skeletal muscle (Sherwin et al., 1974).

Insulin-induced phosphorylation of Akt and eNOS in the ETIrs2KO mice was significantly, but not completely, impaired by endothelial Irs2 deficiency (Figure 2D), suggesting the important role of both Irs2 and Irs1 in this signaling in the endothelial cells. In fact, phosphorylation of Akt and eNOS was completely abrogated in the ETIrs1/2DKO mice (Figure 3I). Thus, in the physiological state, it is likely that insulin-stimulated Irs1-mediated Akt activates eNOS in proportion to the amount of eNOS protein available in these mice.

In this study, we found that endothelial insulin signaling mediates insulin-stimulated capillary recruitment and increase of interstitial insulin concentrations and, as a consequence, facilitates glucose uptake by the skeletal muscle. Skeletal muscle insulin resistance may be caused by impaired insulin signaling not only in the myocytes but also in the endothelial cells. Taken together, treatment directed at improving insulin signaling in the endothelial cells as well as myocytes may serve as a therapeutic strategy for ameliorating skeletal muscle insulin resistance.

EXPERIMENTAL PROCEDURES

Mice

ETIrs1KO or ETIrs2KO mice were generated by mating $Irs1^{lox/+}$ or $Irs2^{lox/+}$ female mice (Kubota et al., 2008) with transgenic mice expressing Cre under control of the murine Tie2 promoter (Tie2-Cre mice) (Kisanuki et al., 2001). The $Irs1^{lox/+}$:Tie2-Cre or $Irs2^{lox/+}$:Tie2-Cre male offspring were then crossed with $Irs1^{lox/+}$ or $Irs2^{lox/+}$ female mice to obtain WT ($Irs1^{+/+}$), Tie2-Cre ($Irs1^{+/+}$:Tie2-Cre), control ($Irs1^{lox/lox}$), and ETIrs1KO ($Irs1^{lox/lox}$:Tie2-Cre) mice, or WT ($Irs2^{+/+}$), Tie2-Cre ($Irs2^{+/+}$:Tie2-Cre), control ($Irs2^{lox/lox}$), and ETIrs2KO ($Irs2^{lox/lox}$:Tie2-Cre) mice, respectively. To generate endothelial-specific Irs1/Irs2 double-knockout (ETIrs1/2DKO) mice, $Irs1^{lox/+}$:Tie2-Cre or $Irs2^{lox/+}$:Tie2-Cre male mice were crossed with $Irs2^{lox/+}$ or $Irs1^{lox/+}$ female mice, and the resultant $Irs1^{lox/+}/Irs2^{lox/+}$:Tie2-Cre male mice were crossed with $Irs1^{lox/+}/Irs2^{lox/+}$ female mice. $Irs1^{lox/lox}/Irs2^{lox/lox}$ mice were used as the control for ETIrs1/2DKO mice. Only male littermates were used for this study; we did not use the female Tie2-Cre, $Irs1^{lox/+}$:Tie2-Cre, $Irs2^{lox/+}$:Tie2-Cre, $Irs1^{lox/+}/Irs2^{lox/+}$:Tie2-Cre, ETIrs1KO, ETIrs2KO, or ETIrs1/2DKO mice for breeding. Further information is provided in the Supplemental Information. The animal care and experimental procedures used in this study were approved by the Animal Care Committee of the University of Tokyo.

Capillary Blood Volume

The capillary blood volume was measured by contrast-enhanced ultrasound, as described previously (Vincent et al., 2004), with some modifications. The hindlimb muscles were imaged in the short axis using a 40 MHz transducer (RMV 704) connected to an ultrasound system (Vevo 770; VISUALSONICS Inc.). Sonazoid (Daiichi Sankyo Corporation) was infused into the animals, which were divided into three groups for the measurements at 0, 10, and 60 min after the hyperinsulinemic-euglycemic clamp, a high-power ultrasound with a frequency of 1MHz was applied to the lower leg muscles, and images were collected for 30 s to assess the enhancement. The ultrasound intensity in decibels within the region of interest was converted to the acoustic intensity after background subtraction using 0.5 s ultrasound images, and the microvascular volume, fill rate constant, and capillary blood volume were calculated according to the equation $y = A(1 - e^{-\beta t})$. Further information is provided in the Supplemental Information.

Interstitial Concentrations of Insulin in the Skeletal Muscle

Muscle microdialysis was performed in the hindlimb muscles using a 4 mm microdialysis tubing (CMA-20) at the rate of 0.3 μl/min. We conducted calibration using the no-net flux technique described previously (Jansson et al., 1993), with slight modifications. Briefly, four known concentrations of insulin (0 ng/ml, 0.5 ng/ml, 1 ng/ml, and 1.5 ng/ml) above and below the expected concentration in the skeletal muscle were used. The insulin solutions were added to the perfusate, and the net changes in the concentrations of the analytes in the dialysate were recorded ($insulin_{out} - insulin_{in}$ = net change). Regression analysis yielded a linear relationship between the concentrations in the perfusates and the dialysates. The intercept with the x axis indicates the insulin concentrations in the perfusate at equilibrium with the surrounding medium, and the slope of the line yields the dialysis recovery by the no-net flux technique. The insulin concentrations in the interstitial fluid were calculated from the dialysis recovery by the no-net flux technique and the in vivo dialysate insulin concentration, as described previously (Sjostrand et al., 2002).

Endothelial Cell Culture

The aorta was dissected out from the aortic arch to the abdominal aorta and immersed in 10% FBS-DMEM containing 1000 U/ml heparin. A 24-gauge cannula was inserted into the proximal portion of the aorta. The other side was tied, and the lumen was filled with a solution of collagenase type II (2 mg/ml, dissolved in serum-free DMEM). After incubation at 37°C for 45 min, the endothelial cells were removed from the aorta by flushing with 5 ml of DMEM containing 10% FBS and cultured in a 35 mm collagen type 1-coated dish. Further information is provided in the Supplemental Information.

Hyperinsulinemic-Euglycemic Clamp

An infusion catheter was inserted into the right jugular vein of the mice, as described previously (Kubota et al., 2008), with some modifications. 1% glucose ([6,6-$^2H_2$]glucose [Sigma]) was infused intravenously, and after a 90 min basal period a blood sample was collected from the tail tip for determination of the basal glucose specific activity. To measure the GIR, a primed-continuous infusion of insulin (Humulin R; Lilly) was administered and the blood glucose concentration was maintained at approximately 120 mg/dl by the administration of glucose (5 g of glucose/10 ml enriched to about 20% with [6,6-$^2H_2$]glucose [Sigma]) for 60 or 120 min. Blood samples (20 μl) were obtained for 15 or 30 min before the end of the hyperinsulinemic-euglycemic clamp. Thereafter, the Rd was calculated according to non-steady-state equations, and the EGP was calculated as the difference between the Rd values and the exogenous GIR. Further information is provided in the Supplemental Information.

Statistical Analysis

Values were expressed as means ± SEM. Student's t test was used for statistical analysis of the differences between two groups, and the statistical significance of differences among multiple groups was determined by ANOVA.

SUPPLEMENTAL INFORMATION

Supplemental Information includes six figures, one movie, Supplemental Experimental Procedures, and Supplemental References and can be found with this article at doi:10.1016/j.cmet.2011.01.018.

ACKNOWLEDGMENTS

We thank Namiko Okajima-Kasuga, Sayaka Sasamoto, Kousuke Yokota, Miyoko Suzuki-Nakazawa, Masahiro Nakamaru, Michiko Kato, Tomoko Asano, Eishin Hirata, Eri Yoshida-Nagata, Ayumi Nagano, Miharu Nakashima, Ritsuko Fujita, and Hiroshi Chiyonobu for their technical assistance and care of the animals. This work was supported by a grant for CREST from the Japan Science and Technology Corporation; a grant for Promotion of Fundamental Studies in Health Science from the Organization for Pharmaceutical Safety and Research; a grant for TSBMI from the Ministry of Education, Culture, Sports, Science and Technology of Japan; a Grant-in-Aid for Scientific Research in Priority Areas (A) (16209030), (A) (18209033), and (S) (20229008) from the Ministry of Education, Culture, Sports, Science, and Technology of Japan (to T. Kadowaki); and a Grant-in-Aid for Scientific Research in Priority Areas (C) (19591037) and (B) (21390279) from the Ministry of Education, Culture, Sports, Science, and Technology of Japan (to N.K.).

Received: May 10, 2010
Revised: August 13, 2010
Accepted: January 24, 2011
Published: March 1, 2011

REFERENCES

Aird, W.C. (2007). Phenotypic heterogeneity of the endothelium. I. Structure, function, and mechanisms. Circ. Res. *100*, 158–173.

Barrett, E.J., Eggleston, E.M., Inyard, A.C., Wang, H., Li, G., Chai, W., and Liu, Z. (2009). The vascular actions of insulin control its delivery to muscle and regulate the rate-limiting step in skeletal muscle insulin action. Diabetologia *52*, 752–764.

Bergman, R.N. (1989). Lilly Lecture: toward physiological understanding of glucose tolerance: minimal-model approach. Diabetes *38*, 1512–1527.

Brüning, J.C., Michael, M.D., Winnary, J.N., Hayashi, T., Hörsch, D., Accili, D., Goodyear, L.J., and Kahn, C.R. (1998). A muscle-specific insulin receptor knockout exhibits features of the metabolic syndrome of NIDDM without altering glucose tolerance. Mol. Cell *2*, 559–569.

Chiu, J.D., Richey, J.M., Harrison, L.N., Zuniga, E., Kolk, C.M., Kirkman, E., Ellmerer, M., and Bergman, R.N. (2008). Direct administration of insulin into skeletal muscle reveals that the transport of insulin across the capillary endothelium limits the time course of insulin to activate glucose disposal. Diabetes *57*, 828–835.

Clark, M.G. (2008). Impaired microvascular perfusion: a consequence of vascular dysfunction and a potential cause of insulin resistance in muscle. Am. J. Physiol. Endocrinol. Metab. *295*, E732–E750.

DeFronzo, R.A., Tobin, J.D., and Andres, R. (1979). Glucose clamp technique: a method for quantifying insulin secretion and resistance. Am. J. Physiol. *237*, E214–E223.

Ellmerer, M., Hamilton-Wessler, M., Kim, S.P., Huecking, K., Kirkman, E., Chiu, J., Richey, J., and Bergman, R.N. (2006). Reduced access to insulin-sensitive tissues in dogs with obesity secondary to increased fat intake. Diabetes *55*, 1769–1775.

Hamilton-Wessler, M., Ader, M., Dea, M.K., Moore, D., Loftager, M., Markussen, J., and Bergman, R.N. (2002). Mode of transcapillary transport of insulin and insulin analog NN304 in dog hindlimb: evidence for passive diffusion. Diabetes *51*, 574–582.

Jansson, P.A., Fowelin, J.P., von Schenck, H.P., Smith, U.P., and Lönnroth, P.N. (1993). Measurement by microdialysis of the insulin concentration in subcutaneous interstitial fluid. Importance of the endothelial barrier for insulin. Diabetes *42*, 1469–1473.

Jiang, Z.Y., Lin, Y.W., Clemont, A., Feener, E.P., Hein, K.D., Igarashi, M., Yamauchi, T., White, M.F., and King, G.L. (1999). Characterization of selective resistance to insulin signaling in the vasculature of obese Zucker (fa/fa) rats. J. Clin. Invest. *104*, 447–457.

Kainoh, M., Maruyama, I., Nishio, S., and Nakadate, T. (1991). Enhancement by beraprost sodium, a stable analogue of prostacyclin, in thrombomodulin expression on membrane surface of cultured vascular endothelial cells via increase in cyclic AMP level. Biochem. Pharmacol. *41*, 1135–1140.

Karnieli, E., Zarnowski, M.J., Hissin, P.J., Simpson, I.A., Salans, L.B., and Cushman, S.W. (1981). Insulin-stimulated translocation of glucose transport systems in the isolated rat adipose cell. Time course, reversal, insulin concentration dependency, and relationship to glucose transport activity. J. Biol. Chem. *256*, 4772–4777.

Keske, M.A., Clerk, L.H., Price, W.J., Jahn, L.A., and Barrett, E.J. (2009). Obesity blunts microvascular recruitment in human forearm muscle after a mixed meal. Diabetes Care *32*, 1672–1677.

Kisanuki, Y.Y., Hammer, R.E., Miyazaki, J., Williams, S.C., Richardson, J.A., and Yanagisawa, M. (2001). Tie2-Cre transgenic mice: a new model for endothelial cell-lineage analysis in vivo. Dev. Biol. *230*, 230–242.

Kubota, T., Kubota, N., Moroi, M., Terauchi, Y., Kobayashi, T., Kamata, K., Suzuki, R., Tobe, K., Namiki, A., Aizawa, S., et al. (2003). Lack of insulin receptor substrate-2 causes progressive neointima formation in response to vessel injury. Circulation *107*, 3073–3080.

Kubota, N., Kubota, T., Itoh, S., Kumagai, H., Kozono, H., Takamoto, I., Mineyama, T., Ogata, H., Tokuyama, K., Ohsugi, M., et al. (2008). Dynamic functional relay between insulin receptor substrate 1 and 2 in hepatic insulin signaling during fasting and feeding. Cell Metab. *8*, 49–64.

Long, Y.C., and Zierath, J.R. (2008). Influence of AMP-activated protein kinase and calcineurin on metabolic networks in skeletal muscle. Am. J. Physiol. Endocrinol. Metab. *295*, E545–E552.

Miles, P.D., Levisetti, M., Reichart, D., Khoursheed, M., Moossa, A.R., and Olefsky, J.M. (1995). Kinetics of insulin action in vivo. Identification of rate limiting steps. Diabetes *44*, 947–953.

Muniyappa, R., and Quon, M.J. (2007). Insulin action and insulin resistance in vascular endothelium. Curr. Opin. Clin. Nutr. Metab. Care *10*, 523–530.

Niwano, K., Arai, M., Tomaru, K., Uchiyama, T., Ohyama, Y., and Kurabayashi, M. (2003). Transcriptional stimulation of the eNOS gene by the stable prostacyclin analogue beraprost is mediated through cAMP-responsive element in vascular endothelial cells: close link between PGI2 signal and NO pathways. Circ. Res. *93*, 523–530.

Nolan, J.J., Ludvik, B., Baloga, J., Reichart, D., and Olefsky, J.M. (1997). Mechanisms of the kinetic defect in insulin action in obesity and NIDDM. Diabetes *46*, 994–1000.

Petersen, K.F., Dufour, S., Befroy, D., Garcia, R., and Shulman, G.I. (2004). Impaired mitochondrial activity in the insulin-resistant offspring of patients with type 2 diabetes. N. Engl. J. Med. *350*, 664–671.

Rattigan, S., Clark, M.G., and Barrett, E.J. (1997). Hemodynamic actions of insulin in rat skeletal muscle: evidence for capillary recruitment. Diabetes *46*, 1381–1388.

Sherwin, R.S., Kramer, K.J., Tobin, J.D., Insel, P.A., Liljenquist, J.E., Berman, M., and Andres, R. (1974). A model of the kinetics of insulin in man. J. Clin. Invest. *53*, 1481–1492.

Sjostrand, M., Gudbjornsdottir, S., Holmang, A., Lonn, L., Strindberg, L., and Lönnroth, P. (2002). Delayed transcapillary transport of insulin to muscle interstitial fluid in obese subjects. Diabetes *51*, 2742–2748.

Vicent, D., Ilany, J., Kondo, T., Naruse, K., Fisher, S.J., Kisanuki, Y.Y., Bursell, S., Yanagisawa, M., King, G.L., and Kahn, C.R. (2003). The role of endothelial insulin signaling in the regulation of vascular tone and insulin resistance. J. Clin. Invest. *111*, 1373–1380.

Vincent, M.A., Clerk, L.H., Lindner, J.R., Klibanov, A.L., Clark, M.G., Rattigan, S., and Barrett, E.J. (2004). Microvascular recruitment is an early insulin effect that regulates skeletal muscle glucose uptake in vivo. Diabetes *53*, 1418–1423.

Vincent, M.A., Clerk, L.H., Rattigan, S., Clark, M.G., and Barrett, E.J. (2005). Active role for the vasculature in the delivery of insulin to skeletal muscle. Clin. Exp. Pharmacol. Physiol. *32*, 302–307.

Wallis, M.G., Wheatley, C.M., Rattigan, S., Barrett, E.J., Clark, A.D.H., and Clark, M.G. (2002). Insulin-mediated hemodynamic changes are impaired in muscle of Zucker obese rats. Diabetes *51*, 3492–3498.

Wang, H., Wang, A.X., Liu, Z., and Barrett, E.J. (2008). Insulin signaling stimulates insulin transport by bovine aortic endothelial cells. Diabetes *57*, 540–547.

White, M.F., and Kahn, C.R. (1994). The insulin signaling system. J. Biol. Chem. *269*, 1–4.

Yang, Y.J., Hope, I.D., Ader, M., and Bergman, R.N. (1989). Insulin transport across capillaries is rate limiting for insulin action in dogs. J. Clin. Invest. *84*, 1620–1628.

Available online at www.sciencedirect.com
ScienceDirect
Metabolism Clinical and Experimental 60 (2011) 617–628
Metabolism
Clinical and Experimental
www.metabolismjournal.com

Ezetimibe decreases SREBP-1c expression in liver and reverses hepatic insulin resistance in mice fed a high-fat diet

Tomonori Muraoka[a], Kazutaka Aoki[a], Tomoyuki Iwasaki[a], Kazuaki Shinoda[a], Akinobu Nakamura[a], Hiroyuki Aburatani[b], Shuuichi Mori[c], Kumpei Tokuyama[c], Naoto Kubota[d], Takashi Kadowaki[d], Yasuo Terauchi[a,*]

[a]*Department of Endocrinology and Metabolism, Yokohama City University Graduate School of Medicine, Yokohama 236-0004, Japan*
[b]*Genome Science Division, Research Center for Advanced Science and Technology, University of Tokyo, Tokyo 153-8904, Japan*
[c]*Graduate School of Comprehensive Human Sciences, University of Tsukuba, Tsukuba 305-0006, Japan*
[d]*Department of Metabolic Diseases, Graduate School of Medicine, University of Tokyo, Tokyo 113-8655, Japan*

Received 21 December 2009; accepted 7 June 2010

Abstract

Ezetimibe inhibits intestinal cholesterol absorption, thereby reducing serum cholesterol. Recent studies suggest that ezetimibe affects liver steatosis and insulin resistance. We investigated the impact of ezetimibe on insulin sensitivity and glucose metabolism in C57BL/6 mice. We analyzed 4 mouse groups fed the following diets: normal chow (4% fat) for 12 weeks, normal chow for 10 weeks followed by normal chow plus ezetimibe for 2 weeks, high-fat chow (32% fat) for 12 weeks, and high-fat chow for 10 weeks followed by high-fat chow plus ezetimibe for 2 weeks. In the normal chow + ezetimibe group, ezetimibe had no impact on body weight, fat mass, lipid metabolism, liver steatosis, glucose tolerance, or insulin sensitivity. In the high-fat chow + ezetimibe group, ezetimibe had no impact on body weight or fat mass but significantly decreased serum low-density lipoprotein cholesterol, triglyceride, and glutamate pyruvate transaminase levels; liver weight; hepatic triglyceride content; and hepatic cholesterol content and increased the hepatic total bile acid content. In association with increases in IRS-2 and Akt phosphorylation, ezetimibe ameliorated hepatic insulin resistance in the high-fat chow + ezetimibe group, but had no effect on insulin sensitivity in primary cultured hepatocytes. A DNA microarray and Taqman polymerase chain reaction revealed that ezetimibe up-regulated hepatic SREBP2 and SHP expression and down-regulated hepatic SREBP-1c expression. SHP silencing mainly in the liver worsened insulin resistance, and ezetimibe protected against insulin resistance induced by down-regulation of SHP. Ezetimibe down-regulated SREBP-1c in the liver and reversed hepatic insulin resistance in mice fed a high-fat diet.

1. Introduction

Ezetimibe is a novel sterol absorption inhibitor that blocks Niemann-Pick C1-Like 1 (NPC1L1)–mediated cholesterol absorption in the apical brush border membrane of jejunal enterocytes [1]. NPC1L1 null mice were completely resistant to high-cholesterol-diet–induced hypercholesterolemia, with plasma lipoprotein and hepatic cholesterol profiles similar to those of wild-type mice treated with ezetimibe [2]. Ezetimibe prevented lipid-rich-diet–induced increase in biliary cholesterol in hamsters [3]. Recently, potential consequences of ezetimibe relative to metabolism of other nutrients have been investigated. In animal experiments, ezetimibe reversed diet-induced obesity [4,5], liver steatosis [4-7], and insulin resistance [6]. In humans, in addition to the effect of ezetimibe on lowering serum low-density lipoprotein (LDL) cholesterol [8], its potential effects on liver steatosis [9] and insulin resistance [10] have been reported. Nevertheless, the mechanism whereby ezetimibe achieves these favorable effects on insulin sensitivity remains unclear. These circumstances prompted us to investigate the effects of ezetimibe on insulin sensitivity and glucose metabolism using high-fat-diet–induced C57BL/6 obese mice to pursue the possibility of new mechanisms explaining these beneficial effects.

* Corresponding author. Tel.: +81 45 787 2639.
E-mail address: terauchi@yokohama-cu.ac.jp (Y. Terauchi).

0026-0495/$ – see front matter © 2011 Elsevier Inc. All rights reserved.
doi:10.1016/j.metabol.2010.06.008

2. Materials and methods

2.1. Chemicals

Ezetimibe is a novel sterol absorption inhibitor that blocks NPC1L1-mediated cholesterol/phytosterol absorption in the apical brush border membrane of jejunal enterocytes, as described previously [1]. The Schering-Plough Research Institute provided us with ezetimibe.

2.2. Animals and diet protocol

Male C57BL/6 mice (7 weeks of age) (Japan SLC, Shizuoka, Japan) were fed a normal chow diet (Type MF; Oriental Yeast, Tokyo, Japan) for 1 week and were then divided into 4 groups that were each fed a specific diet for the next 12 weeks. We thus analyzed 4 mouse groups, namely, mice fed a normal chow diet for 12 weeks (NC), mice fed a normal chow diet for 10 weeks followed by normal chow diet containing 0.005% wt/wt ezetimibe for 2 weeks (NC + Ez), mice fed a high-fat chow (High-Fat Diet 32; CLEA Japan, Tokyo, Japan) for 12 weeks (HF), and mice fed a high-fat chow for 10 weeks followed by high-fat chow containing 0.005% wt/wt ezetimibe for 2 weeks (HF + Ez). Cholesterol absorption is inhibited by more than 90% at ezetimibe doses of more than 3 mg/kg in apolipoprotein E–knockout mice [11]. The target doses of 0.005% wt/wt ezetimibe mixed in either normal chow or high-fat chow corresponded to a dose of 3 mg/kg body weight in the C57BL/6J mice. The nutrient compositions of the chows are described in Table 1. The mice were given free access to water and food until the start of the experiments. The experiments were approved by the Ethical Committee for Animal Experimentation of Yokohama City Medical University, and the animals were maintained according to standard animal care procedures based on institutional guidelines.

2.3. Measurement of lipids and bile acid

The extraction of lipids from liver tissue was performed as described by Folch et al [12]. Plasma lipoproteins were analyzed using an online dual enzymatic method for the simultaneous quantification of cholesterol and triglycerides (TGs) using high-performance liquid chromatography at Skylight Biotech (Akita, Japan), according to the procedure reported by Usui et al [13]. The total bile acid level in the serum was determined by using enzymatic methods at SRL (Tokyo, Japan). Bile acid in the liver was extracted using the ethanol-thermal method, and the bile acid content was determined using enzymatic methods at Skylight-Biotec according to the procedure reported by Udagawa et al [14] with slight modifications.

Table 1
Nutritional components of Type MF and High-Fat Diet 32

	Type MF	High-Fat Diet 32
Moisture (g/100 g)	7.8	6.9
Content of crude protein (g/100 g)	23.8	25.0
Content of crude fat (g/100 g)	3.7	32.4
Content of crude ash (g/100 g)	6.1	4.0
Content of crude fiber (g/100 g)	3.2	2.9
Nitrogen-free extract (g/100 g)	54.0	28.8
Cholesterol content (mg/100 g)	75	12.9
Calorie (kcal/100 g)	357	507.6

2.4. Histology of the liver

To study the liver histology, the livers were dissected and fixed in buffered neutral formalin (10%). The fixed-tissue blocks were embedded in paraffin, and 4-μm paraffin sections were stained using the standard hematoxylin and eosin staining procedure.

2.5. Oral glucose tolerance test

Each group of mice was given an oral glucose tolerance test (1.5 mg of glucose per gram of body weight after 18 hours of fasting). The glucose levels were measured at 0, 15, 30, 60, and 120 minutes using whole blood obtained from the tail vein and a portable blood glucose analyzer (Glutest Neo; Sanwa Chemical, Nagoya, Japan); the insulin levels were measured at 0, 15, and 30 minutes using an enzyme-linked immunosorbent assay kit (Morinaga, Kanagawa, Japan), as previously described [15].

2.6. Insulin tolerance test

Each group of mice was given an insulin tolerance test. Mice were given free access to food and were then intraperitoneally injected with 0.75 mU of insulin per gram of body weight. The glucose levels were then measured at 0, 15, 30, 60, and 120 minutes using whole blood obtained from the tail vein and a portable blood glucose analyzer (Glutest Neo).

2.7. Hyperinsulinemic-euglycemic clamp study

Clamp studies were performed as described previously [16-18]. Briefly, 2 to 3 days before the study, an infusion catheter was inserted into the right jugular vein under general anesthesia with sodium pentobarbital. Studies were performed on mice under conscious and unstressed conditions after a 6-hour fast. A primed continuous infusion of insulin (Humulin R; Eli Lilly and Company, Indianapolis, IN, USA) was given (5.0 mU/[kg min]), and the blood glucose concentration, monitored every 5 minutes, was maintained at 120 mg/dL through the administration of glucose (5 g of glucose per 10 mL enriched to approximately 20% with [6,6-2H2]glucose [Sigma, Tokyo, Japan]) for 120 minutes. Blood was sampled via tail tip bleeds at 90, 105, and 120 minutes to determine the rate of glucose disappearance (Rd). Rd was calculated using non–steady-state equations, and endogenous glucose production (EGP) was calculated as the difference between Rd and the exogenous glucose infusion rate (GIR).

2.8. In vivo IRS-1/2 and Akt phosphorylation

The monoclonal antiphosphotyrosine antibody (anti-PY), polyclonal anti–IRS-1 antibody (anti–IRS-1), and polyclonal anti–IRS-2 antibody (anti–IRS-2) were purchased from Upstate Biotechnology (Lake Placid, NY, USA). Rabbit polyclonal anti–phospho-Akt antibody (anti-pAkt) recognizing phosphorylated Ser-473 of Akt1 and rabbit anti-Akt antibody (anti-Akt) were purchased from Cell Signaling Technology (Beverly, MA). Mice in the HF and HF + Ez groups were starved for 24 hours, anesthetized with pentobarbital, and injected with 15 units of regular human insulin (Humulin R) or saline into the inferior vena cava. Seventy seconds later, the livers were excised and homogenized in ice cold buffer A (25 mmol/L Tris-HCl [pH 7.4], 10 mmol/L Na_3VO_4, 10 mmol/L NaPPi, 100 mmol/L NaF, 10 mmol/L EDTA, 10 mmol/L EGTA, and 1 mmol/L phenylmethylsulfonyl fluoride). Lysates were prepared by centrifugation (15 000 rpm, 20 minutes, 4°C). Immunoprecipitation analyses for either IRS-1 or IRS-2 and Western blot analyses for Akt and pAkt were then performed. To detect the immunoprecipitation of either IRS-1 or IRS-2 and their phosphorylation, liver extracts were incubated with specific antibodies against either IRS-1 or IRS-2 at 4°C overnight and then with protein G–Sepharose for 2 hours at 4°C. After washing 3 times with buffer A, the immunocomplexes were resolved on 7% sodium dodecyl sulfate polyacrylamide gel electrophoresis. The phosphorylated or total protein was then analyzed using immunoblotting with specific antibodies against either IRS-1 or IRS-2 and a phosphotyrosine antibody. Akt activity was expressed as the ratio of the intensity of pAkt to Akt.

2.9. RNA preparation and microarray analysis of messenger RNA levels in the liver

Mice in the HF and HF + Ez groups were subjected to fasting for 24 hours. Total RNA was prepared from portions of the liver using Isogen Reagent (NipponGene, Tokyo, Japan) according to the manufacturer's instructions. RNA was further purified using a NucleoSpin RNA II column (Macherey-Nagel, Duren, Germany), and RNA quality was assessed after electrophoresis in a 1% agarose gel. GeneChip assays were then performed, as previously described [18]. Briefly, double-strand standard complementary DNA with a T7 promoter was synthesized from 5 μg of total RNA using the SuperScript choice system (Invitrogen-Life Technologies, Carlsbad, CA, USA). Approximately 50 μg of biotin-labeled complementary RNA was synthesized using in vitro transcription with T7 polymerase. After purification and fragmentation, complementary RNA was hybridized to the oligonucleotide microarray (Mouse Genome 430 2.0 Array; Affymetrix, Santa Clara, CA, USA). The scanned images were interpreted using GeneChip Operating Software 1.4 (Affymetrix) to generate a score representing the expression level of each gene. The microarray data have been deposited in the Gene Expression Omnibus public database.

2.10. Taqman polymerase chain reaction

Total RNA was prepared as mentioned above. The messenger RNA levels in the liver were quantitatively analyzed using fluorescence-based reverse transcriptase polymerase chain reaction (PCR). The reverse transcription mixture was amplified using specific primers and an ABI Prism 7500 sequence detector equipped with a thermocycler. The primers were purchased from Applied Biosystems (Foster City, CA). The relative expression levels were compared after normalization to β-actin [19].

2.11. Establishment of primary cultured hepatocytes and in vitro Akt phosphorylation experiment

Mice were anesthetized by the intraperitoneal administration of pentobarbital (40 mg/kg). Mouse hepatocytes were then isolated by the perfusion of collagenase through the abdominal vein, as previously described [20,21]. Briefly, the liver was perfused with a calcium-free Hanks HEPES buffer containing EGTA, followed by perfusion with Hanks HEPES buffer containing collagenase (0.1%). The "softened" liver was then excised, and the hepatocytes were separated from the connective tissue by filtering through macroporous filters (150 mesh; Ikemoto Scientific Technology, Tokyo, Japan). To remove nonparenchymal cells, the hepatocytes were washed with Williams medium E in Hanks buffer by repeated centrifugation for 3 minutes (each time) at 50*g*. The cell pellet was resuspended in Williams medium E containing streptomycin (100 μg/mL), penicillin (100 U/mL), and fetal bovine serum (10%); and the cell suspension was seeded into 24-well collagen-coated plates. The cells were cultured at 37°C under 5% CO_2 humidified air. After overnight incubation, the cells were washed with phosphate-buffered saline (PBS); and the buffer was changed to glucose-free Hanks solution, a substrate for gluconeogenesis, as previously described [22]. The cells were washed with PBS and then treated with ezetimibe (25 μmol/L) or dimethyl sulfoxide in medium for 48 hours, followed by treatment with insulin (10 nmol/L) or PBS for 5 minutes, as previously described [4]. The cells were lysed and subjected to Western blot analysis, as described above. Akt activity was expressed as the ratio of the intensity of pAkt to Akt.

2.12. Preparations of small interfering RNA and small interfering RNA treatment

Synthetic small interfering RNA (siRNA) was purchased from Takara Bio (Shiga, Japan). Sequences of the sense and anti-sense strands of siRNA were 5′-CGGACUUCCUUGCUUUGGATT-3′ and 5′-UCCAAAGCAAGGAACUCGTT-3′, respectively. Synthetic siRNAs were delivered in vivo using a modified hydrodynamic transfection method [23]. Mice fed a high-fat chow for 10 weeks were fasted 12 hours before hydrodynamic injection. Fifty micrograms siRNA dissolved in 2 mL Ringer buffer was rapidly injected into the tail vein, and then mice were immediately refed either

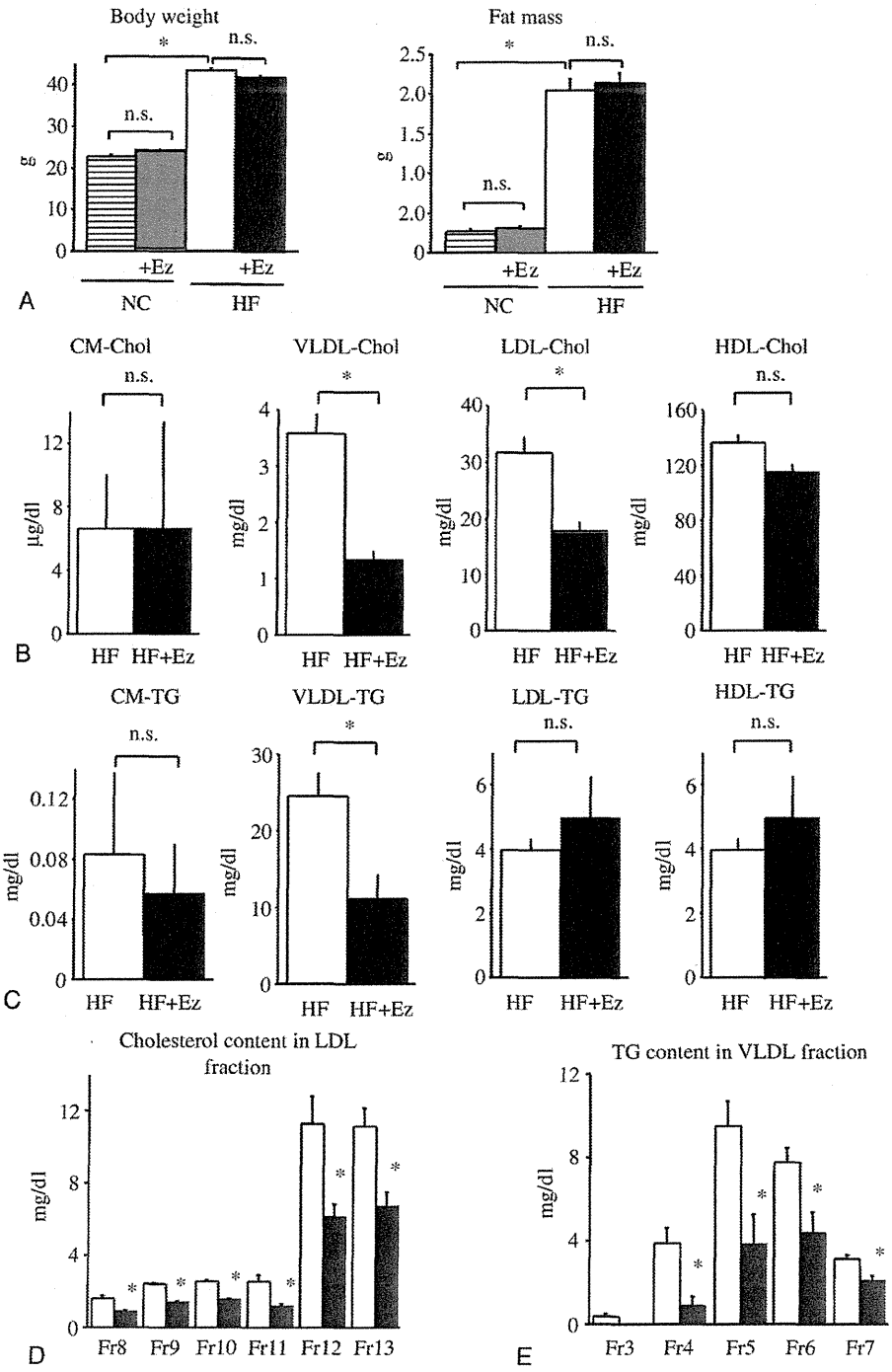

Fig. 1. Impact of ezetimibe on body weight, fat mass, and lipid metabolism in mice fed either a normal chow diet or a high-fat diet. A, Body weight and epididymal fat weight after 12 weeks on either diet. Mice were fed NC (striped bar), NC + Ez (gray bar), HF (open bar), or HF + Ez (filled bar) (n = 9-13). B, Cholesterol content in each lipoprotein in the HF (open bar) and HF + Ez (filled bar) groups (n = 6). The cholesterol contents in chylomicron, VLDL, LDL, and high-density lipoprotein were determined. C, Triglyceride content in each lipoprotein in the HF and HF + Ez groups (n = 6). The TG contents in chylomicron, VLDL, LDL, and high-density lipoprotein were determined. D, Cholesterol content in LDL fraction further analyzed in 6 subfractions according to particle size (n = 6). E, Triglyceride content in VLDL further analyzed in 6 subfractions according to particle size (n = 6). Values are the means ± SE. *$P < .05$. CM indicates chylomicron; HDL, high-density lipoprotein.

high-fat chow or high-fat chow containing 0.005% wt/wt ezetimibe for 2 weeks. Body weight, fat mass, liver weight, and fasting plasma glucose were measured at the indicated time points after injection; and total RNA was prepared. Insulin tolerance test was conducted at the indicated time point: Mice were given free access to food and were then intraperitoneally injected with 1.5 mU of insulin per gram of body weight.

2.13. Statistical analysis

Results were expressed as the means ± SEM. Statistical differences were analyzed using the Student *t* test for unpaired comparisons and Scheffe test for comparisons among the 3 or 4 groups of mice using StatView software, version 5.0 (SAS, Cary, NC). A P value < .05 was considered statistically significant.

3. Results

3.1. No impact of ezetimibe on body weight or fat mass in mice fed a normal chow or high-fat diet

A high-fat diet treatment significantly increased body weight and fat mass, but the 2-week administration of

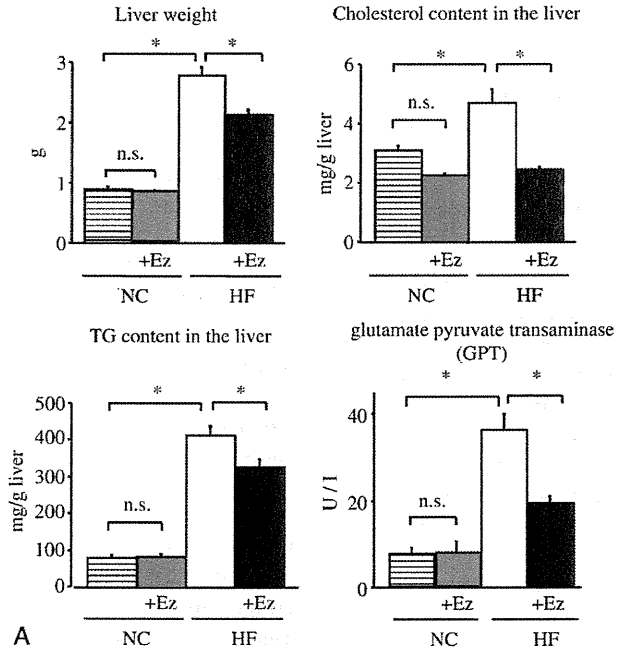

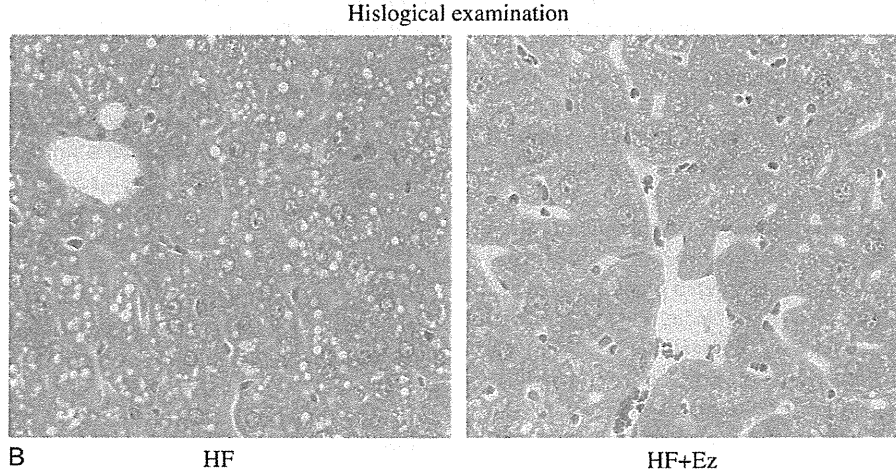

Fig. 2. Impact of ezetimibe on liver steatosis in mice fed a normal chow diet or a high-fat diet. A, Liver weights in the NC, NC + Ez, HF, and HF + Ez groups (n = 9-13). The TG contents (n = 9-10) and cholesterol contents (n = 5) in the livers of the NC, NC + Ez, HF, and HF + Ez groups are shown. The GPT levels in the NC, NC + Ez, HF, and HF + Ez groups are also shown (n = 9-13). B, Histologic analysis of liver samples stained with hematoxylin and eosin (100×) in the HF and HF + Ez groups. The values are the means ± SE. *P < .05.

ezetimibe had no impact on body weight or fat mass in mice fed either a high-fat diet or a normal chow diet (Fig. 1A).

3.2. Impact of ezetimibe on lipid metabolism in mice fed a normal chow or high-fat diet

A high-fat diet significantly increased the serum LDL cholesterol level, but not the TG level (data not shown). Among animals fed a high-fat diet, the addition of ezetimibe significantly lowered the serum cholesterol in the very low-density lipoprotein (VLDL) and LDL fractions, and TG in the VLDL fraction (Fig. 1B, C). The reduction in the cholesterol content was prominent in the VLDL and LDL fractions, especially for smaller-sized particles corresponding to small dense LDL (Fig. 1D). The reduction in the TG content was also prominent in the VLDL and LDL fractions, especially for larger-sized particles corresponding to VLDL1 (Fig. 1E). By contrast, the total cholesterol, LDL cholesterol, and TG levels were unchanged between the NC and NC + Ez groups (data not shown).

3.3. Impact of ezetimibe on liver steatosis in mice fed a normal chow or high-fat diet

A high-fat diet significantly increased the liver weight, the TG content in the liver, the cholesterol content in the liver, and the glutamate pyruvate transaminase (GPT) level. Among animals fed a high-fat diet, ezetimibe significantly lowered the liver weight, the TG content in the liver, and the cholesterol content in the liver, although no significant effects on body weight or visceral fat accumulation were observed (Fig. 2A). Histologic examination revealed that ezetimibe improved high-fat-diet–induced lipid accumulation in the liver (Fig. 2B). In contrast, the liver weights, GPT levels, and hepatic TG contents were unchanged between the NC and NC + Ez groups.

3.4. Impact of ezetimibe on glucose tolerance and insulin sensitivity in mice fed a normal chow or high-fat diet

A high-fat diet significantly increased the fasting plasma glucose level. Ezetimibe had no impact on the fasting plasma glucose level of mice fed either a high-fat diet or a normal chow diet. Of note, ezetimibe significantly strengthened the hypoglycemic effect of insulin in animals fed a high-fat diet, whereas it did not affect insulin sensitivity in animals fed a normal chow diet (Fig. 3A). We next performed a glucose tolerance test. A high-fat diet exacerbated glucose tolerance, compared with a normal chow diet. Under our experimental conditions, ezetimibe had no impact on fasting and postprandial glucose levels in mice fed either a high-fat diet or a normal chow diet but reduced the serum insulin levels after glucose loading in animals fed a high-fat diet (Fig. 3B). This result was consistent with the increase in insulin sensitivity caused by ezetimibe in animals fed a high-fat diet. A hyperinsulinemic-euglycemic clamp study revealed that the administration of ezetimibe improved the GIR and EGP in the liver but did not improve peripheral insulin sensitivity (Fig. 3C). Because hyperinsulinemic-euglycemic clamp studies have been used to investigate insulin-suppressive effect on hepatic glucose production under hyperinsulinemic conditions [24], our results (Fig. 3C) suggest that ezetimibe reverses hepatic insulin resistance under hyperinsulinemic conditions rather than under basal conditions (low concentration of insulin).

To confirm the increased insulin action in mice treated with ezetimibe, we injected insulin into the inferior vena cava and examined insulin-stimulated IRS-1, IRS-2, and Akt phosphorylation. Under basal conditions (low concentration of insulin), phosphorylation of these molecules was indistinguishable between the 2 mouse groups. Ezetimibe significantly enhanced insulin-stimulated Akt phosphorylation and tended to increase insulin-stimulated IRS-2 phosphorylation, although the latter change was not significant (Fig. 3D). Thus, in animals fed a high-fat diet, ezetimibe improved hepatic insulin resistance in association with an increase in IRS-2 and Akt phosphorylation and suppressed hepatic glucose production under hyperinsulinemic conditions.

3.5. Impact of ezetimibe on changes in gene expression profiles in the livers of mice fed a high-fat diet

To identify genes that likely affect glucose and lipid metabolism, we performed a DNA microarray. Of the 45,101 genes examined, 609 were significantly overexpressed and 888 were underexpressed in the livers of the HF + Ez group compared with the livers of the HF group. Interestingly, the lower expression of SREBP-1, ACC, SCD-1, CYP7A1, and liver CPT1 and the higher expression of SREBP2, SHP, HMG-CoA synthase, HMG-CoA reductase, LDL receptor, IRS1, and STAT3 were observed in the livers of the HF + Ez group compared with the livers of the HF group (Table 2). A Taqman PCR analysis confirmed the up-regulation of SREBP-2 and SHP and the down-regulation of SREBP-1c in the livers of the HF + Ez group compared with the livers of the HF group (Fig. 4A, B). The expressions of genes involved in fatty acid β-oxidation and inflammatory reactions were mostly unaltered between the HF and HF + Ez groups, except for the expression of CPT-1 (Table 2). Expression of G6Pase was significantly decreased in the HF + Ez group compared with the HF group, but expressions of glucokinase and PEPCK were unaltered between the 2 groups (Fig. 4C).

Expression of SHP was down-regulated and that of SREBP-1c was up-regulated in the livers on the HF diet compared with those on the normal chow (Fig. 4A).

3.6. No impact of ezetimibe on insulin sensitivity in primary cultured hepatocytes

To examine the ability of ezetimibe to ameliorate hepatic insulin resistance directly in vitro, we established primary cultured hepatocytes and examined insulin-stimulated Akt phosphorylation in the presence of 25 μmol/L of ezetimibe

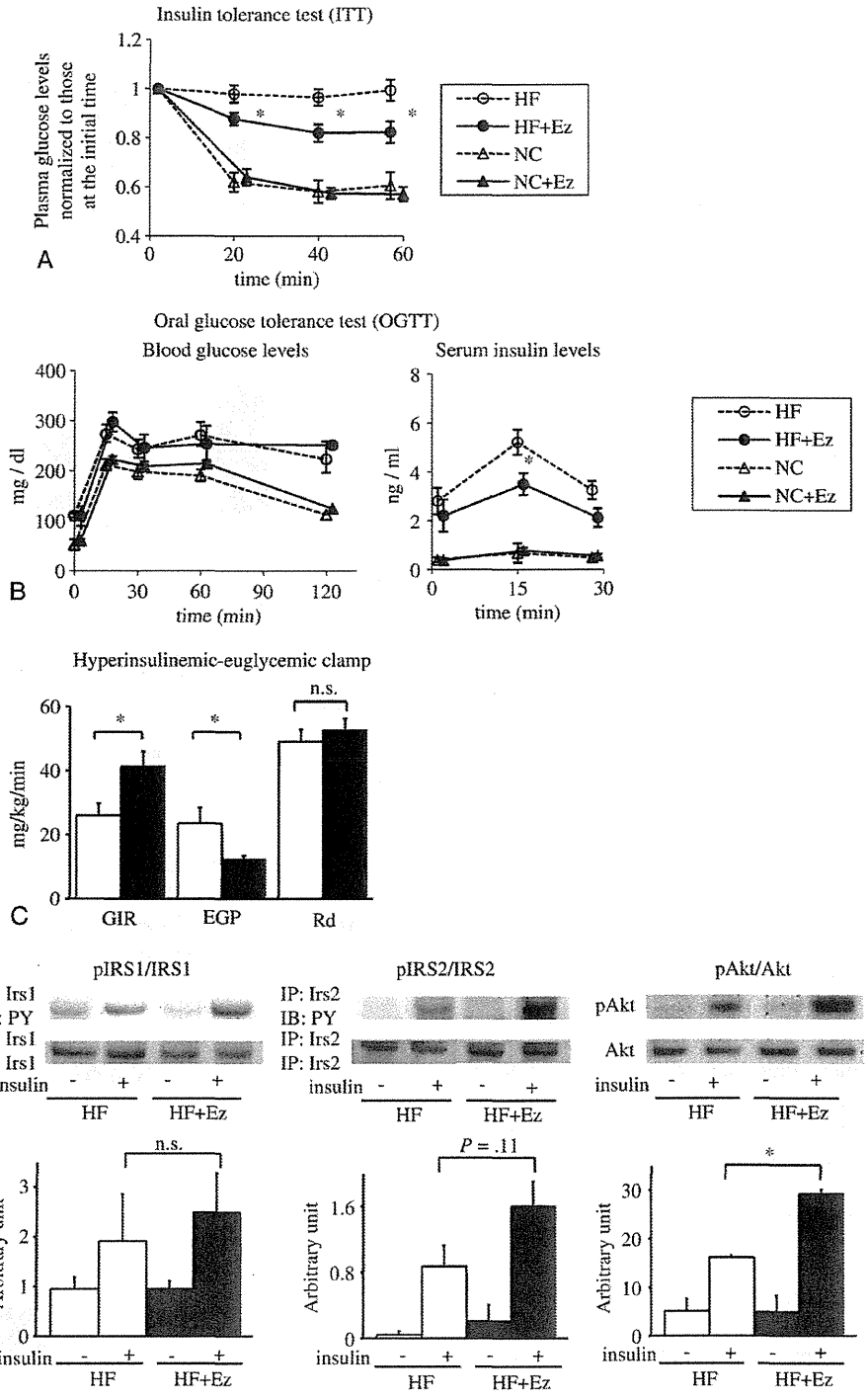

Fig. 3. Impact of ezetimibe on glucose tolerance and insulin sensitivity in mice fed a normal chow or high-fat diet. A, Blood glucose levels during insulin tolerance test in the HF (open circles), HF + Ez (filled circles), NC (open triangles), and NC + Ez (filled triangles) groups (n = 9). B, Blood glucose and plasma insulin levels during an oral glucose tolerance test conducted after 18 hours of fasting in the HF (open circles), HF + Ez (filled circles), NC (open triangles), and NC + Ez (filled triangles) groups (n = 9). C, Glucose infusion rate, EGP, and Rd in the HF (open bar) and HF + Ez (filled bar) groups in a hyperinsulinemic-euglycemic clamp study conducted after 6 hours of fasting (n = 8). D, Insulin-stimulated phosphorylation of Irs1, Irs2, and Akt in the livers of the HF (open bar) and HF + Ez (filled bar) groups (n = 4). The values are the means ± SE. *$P < .05$. HF vs HF + Ez.

Table 2
Changes in gene expression levels in the liver based on a DNA microarray analysis

SREBP pathway		
SREBP1	D	−0.5
SREBP2	I	0.9
Nuclear receptors		
SHP	I	0.5
LXRα, FXR, LRH-1	NS	
Fatty acid and TG biosynthesis		
ACC	D	−0.4
SCD-1	D	−0.5
FAS, ME	NS	
Cholesterol homeostasis and bile acid biosynthesis		
HMG-CoA synthase	I	0.4
HMG-CoA reductase	I	1.4
LDL receptor	I	0.4
CYP7A1	D	−0.9
CYP8B1, ABCA, ABCG5	NS	
Fatty acid β-oxidation		
CPT-1	D	−0.9
MCAD, LCAD	NS	
Insulin signaling		
IRS1	I	0.3
STAT3	I	−1.0
IRS2, CREB, TORC2, CBP, FOXO1, PGC1α	NS	
Inflammatory reactions		
NF-κB, JNK, TNF-α, IKKB, MCP-1, MIP-1α, IL-6	NS	

Log ratios are based on comparisons of HF + Ez vs HF. I indicates increase; D, decrease; NS, no significant change.

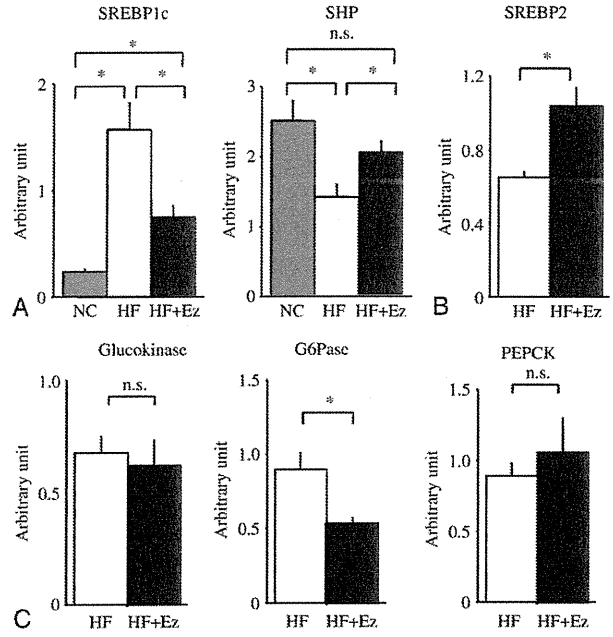

Fig. 4. Impact of ezetimibe on changes in gene expression profiles in the liver. A, Results of Taqman PCR analyses of the expression levels of SREBP-c and SHP in the livers of the NC (gray bar), HF (open bar), and HF + Ez (filled bar) groups (n = 4-6). B, Results of Taqman PCR analyses of the expression levels of SREBP2 in the livers of the HF (open bar) and HF + Ez (filled bar) groups (n = 6). The values are the means ± SE. *$P < .05$. C, Results of Taqman PCR analyses of the expression levels of Gck, G6Pase, and PEPCK in the livers of the HF (open bar) and HF + Ez (filled bar) groups (n = 8-9). The values are the means ± SE. *$P < .05$.

or dimethyl sulfoxide, followed by treatment with 10 nmol/L of insulin. Ezetimibe did not enhance insulin-stimulated Akt phosphorylation in murine cells (Fig. 5), indicating that the improvement in insulin sensitivity induced by ezetimibe in vivo (Fig. 3C, D) cannot be explained by a direct effect on the liver.

3.7. Total bile acid in the serum and liver

The total bile acid concentrations in the serum were very low and indistinguishable among the 4 groups (Fig. 6A). A high-fat diet treatment drastically decreased the total bile acid content in the liver, and ezetimibe significantly increased the total bile acid content in the livers of animals fed a high-fat diet (Fig. 6B).

3.8. RNA interference targeting SHP

To examine the role of SHP in hepatic insulin sensitivity, we performed RNA interference targeting SHP (SHP siRNA). Intravenous injection of siRNA silenced gene expression posttranscriptionally mainly in the liver [25-27] (Fig. 7A). SHP siRNA reduced SHP messenger RNA levels in the liver 24 hours after an injection, but the effects diminished by day 14. SHP siRNA did not significantly affect SREBP-1c expression in the liver under fasting conditions. At day 14, SHP siRNA significantly exacerbated the hypoglycemic effect of insulin in animals fed a high-fat diet (Fig. 7B), whereas it did not affect body weight, fat mass, or liver weight (Fig. 7C). Meanwhile, ezetimibe protected against SHP siRNA-mediated worsening of insulin resistance (Fig. 7B). These results suggest that SHP silencing mainly in the liver worsened insulin resistance and ezetimibe

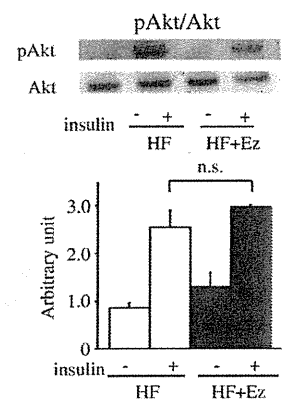

Fig. 5. No impact of ezetimibe on insulin sensitivity in primary cultured hepatocytes. The hepatocytes were incubated with or without ezetimibe (25 μmol/L) for 48 hours, followed by stimulation with insulin (10 nmol/L) for 5 minutes. An immunoblotting analysis was then performed (n = 3). The values are the means ± SE. *$P < .05$.

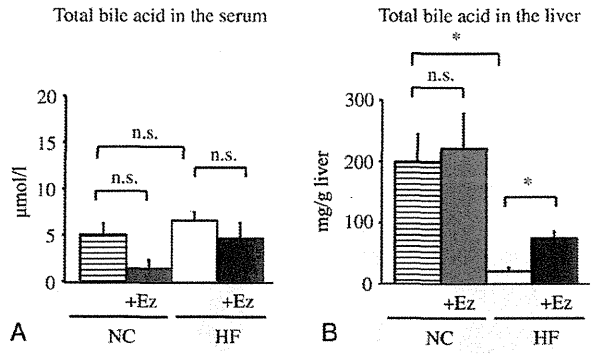

Fig. 6. Total bile acid in the serum and liver. A, Total bile acid levels in the NC, NC + Ez, HF, and HF + Ez groups (n = 5). B, Total bile acid content in the liver of the NC, NC + Ez, HF, and HF + Ez groups (n = 8). The values are the means ± SE. *$P < .05$.

protected mice from insulin resistance associated with the reduction of SHP.

4. Discussion

Previous studies have revealed a potential effect of ezetimibe on insulin sensitivity and glucose metabolism [4,10], but the mechanism responsible for the reversal of insulin resistance has remained unclear. Here, we attempted to reveal the mechanism to explain the effect of ezetimibe on insulin sensitivity and glucose metabolism using C57BL/6 mice with high-fat-diet–induced obesity. We here report 6 findings that link ezetimibe to the reversal of hepatic insulin resistance. First, a euglycemic-hyperinsulinemic clamp study revealed that ezetimibe improved the GIR and EGP in the liver but did not improve peripheral insulin sensitivity (Fig. 3C). Second, ezetimibe improved insulin signaling in the liver, as evidenced by an increase in Akt phosphorylation and a tendency to increase IRS-2 phosphorylation in animals fed a high-fat diet (Fig. 3D). Third, ezetimibe up-regulated SREBP-2 and SHP expression and down-regulated SREBP-1c expression in the liver (Fig. 4). Consistent with these alterations, fatty acid and TG synthesis was suppressed, despite the up-regulation of cholesterol synthesis (Table 2). Fourth, ezetimibe had no impact on insulin sensitivity in primary cultured hepatocytes (Fig. 5). Fifth, a high-fat diet decreased the total bile acid content in the liver; and ezetimibe partially increased it (Fig. 6B). Sixth, SHP silencing mainly in the liver worsened insulin resistance; and ezetimibe protected mice from insulin resistance associated with the reduction of SHP (Fig. 7B). These findings led to our presumption that ezetimibe reverses hepatic insulin resistance via a pathway involving SHP and SREBP-1c in animals fed a high-fat diet.

Unlike rat and human NPC1L1 protein, which is abundantly expressed in the liver, mouse NPC1L1 is predominantly expressed in the intestine [1]. Although it was reported that ezetimibe directly enhanced insulin signaling in HepG2 cells [4], the mechanism seems unlikely to be responsible for the effect of ezetimibe in mice. Thus, NPC1L1 is hardly expressed in murine liver [1]. Consistent with this assumption, ezetimibe had no impact on insulin sensitivity in primary cultured murine hepatocytes (Fig. 5).

Ezetimibe improved insulin signaling in the liver, as evidenced by the increase in Akt phosphorylation, the up-regulation of SHP expression, and the down-regulation of SREBP-1c expressions. What is the molecular link between the up-regulation of SHP, the down-regulation of SREBP-1c, and the reversal of hepatic insulin resistance? The central role of SHP in the process of inhibiting the LXR-SREBP-1c cascade has been reported in studies using SHP knockout mice and pharmacologic experiments [28]. SREBP-1c directly represses the transcription of IRS-2 and inhibits hepatic insulin signaling by inhibiting the downstream PI3K/Akt pathway, leading to a reduction in glycogen synthesis [29]. On the other hand, Yamagata et al [30] reported that bile acids suppress hepatic glucose production in an SHP-dependent fashion, suggesting a potential effect of SHP in the amelioration of insulin resistance via a non–SREBP-1c pathway. This result is consistent with our result that SHP siRNA did not affect SREBP-1c expression in the liver under fasting conditions. However, because expression of SREBP-1c under refed conditions is extremely different from that under fasting conditions [31], further studies are needed to determine whether SHP lowing worsens insulin resistance via SREBP-1c or non–SREBP-1c pathway. Nevertheless, these studies [28-30] support our presumption that ezetimibe reverses hepatic insulin resistance via a pathway involving SHP and SREBP-1c in animals fed a high-fat diet. Furthermore, the presumption is consistent with our result that SHP silencing mainly in the liver worsened insulin resistance and ezetimibe protected mice from SHP-lowing–mediated insulin resistance (Fig. 7B).

It should also be noted that expression of SHP was down-regulated and SREBP-1c was highly up-regulated in the livers of mice fed a high-fat diet compared with the livers of mice fed a normal chow diet. This fact could be one explanation why ezetimibe had no impact on insulin sensitivity in mice fed a normal chow diet, although it reversed hepatic insulin resistance in mice fed a high-fat diet. To sum up, ezetimibe may down-regulate SREBP-1c by up-regulating SHP in the liver and reverses hepatic insulin resistance in mice that have highly expressed SREBP-1c level in the liver.

What is the mechanism for the ezetimibe-induced up-regulation of SHP? SHP is induced in a bile acid–dependent manner in the presence of FXR [32,33] and functions as a direct regulator, consistent with a negative feedback loop in which increased bile acid levels result in a compensatory decrease in the rate of bile acid synthesis [34]. In fact, Watanabe et al [28] demonstrated that bile acids prevent hepatic TG accumulation and VLDL secretion via a pathway involving the up-regulation of SHP and the down-regulation of SREBP-1c in mice fed a high-fat diet. They suggested that

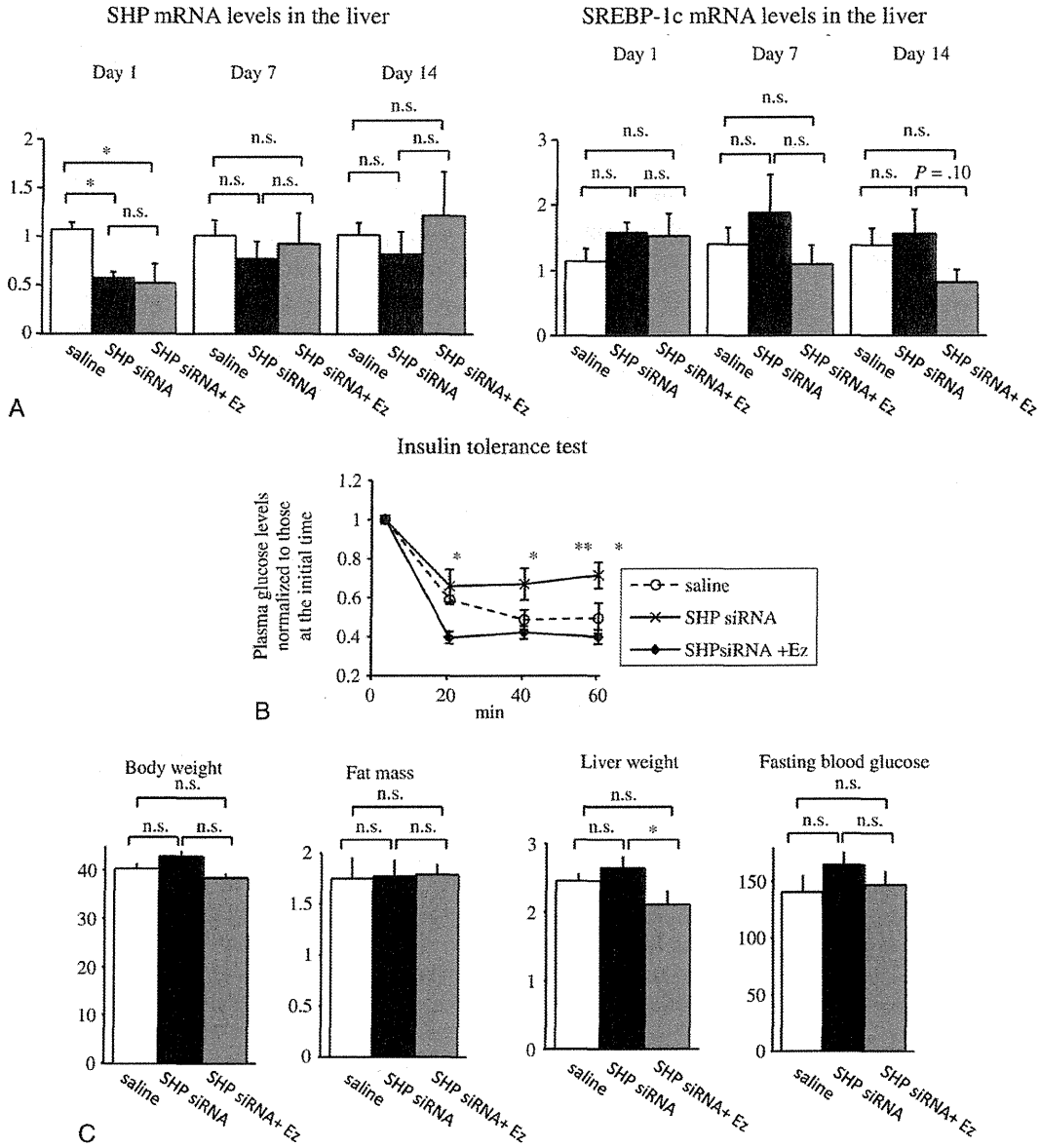

Fig. 7. Impact of intravenous injection of SHP siRNA on body weight, fat mass, liver weight, fasting blood glucose, and insulin sensitivity in mice fed a high-fat diet. A, Results of Taqman PCR analyses of the expression levels of SHP and SREBP-1c in the livers obtained from mice that were injected with saline (open bar), injected with SHP siRNA (filled bar), or treated with ezetimibe after injection of SHP siRNA (gray bar) (n = 3-4). B, Blood glucose levels during insulin tolerance test in mice fed a high-fat diet that were injected with saline (open circle), injected with SHP siRNA (asterisk), or treated with ezetimibe after injection of SHP siRNA (filled square) (n = 4-5). The values are the means ± SE. $*P < .05$ compared with SHP siRNA + Ez. $**P < .05$ compared with saline. C, Body weight, fat mass, liver weight, and fasting blood glucose of mice fed a high-fat diet that were injected with saline (open bar), injected with SHP siRNA (filled bar), or treated with ezetimibe after injection of SHP siRNA (gray bar) (n = 4-5). The values are the means ± SE. $*P < .05$.

a diet-induced increase in the bile acid content in the liver might lead to the up-regulation of SHP. Importantly, ezetimibe increased the total bile acid content in the liver in vivo, despite the down-regulation of CYP7A1 and the absence of any changes in the expressions of CYP8B1, LRH-1, ABCA, or ABCG5 (Table 2). These results suggest that the increased total bile acid content in liver cannot be explained by either an increase in bile acid synthesis or a decrease in the secretion of bile acid in the bile. In fact, it was reported that ezetimibe had no effect on bile acid synthesis in humans or in animal models [3,35,36]. Because the primary effect of ezetimibe is the inhibition of NPC1L1-mediated cholesterol absorption in the intestine, ezetimibe may up-regulate a compensatory uptake of micelle components containing cholesterol, a process that is bile acid dependent but NPC1L1 independent [1,33]. Further research is required

to elucidate how ezetimibe appears to increase the total bile acid content in the liver of C57BL/6 mice fed the types of diets used in the present studies.

What is the relevance of our results to clinical practice in human subjects with insulin resistance? The results of our study indicate that ezetimibe might be effective for ameliorating hepatic insulin resistance under hyperinsulinemic conditions. By contrast, ezetimibe had no substantial impact on insulin sensitivity in animals fed a normal chow diet. This fact suggests that the effectiveness of ezetimibe on improving hepatic insulin sensitivity is dependent on the expression level of SREBP-1c in the liver. Ezetimibe lowered the serum LDL cholesterol level in mice fed a high-fat diet, but failed in mice fed a normal chow diet. The cholesterol content in the normal chow diet was larger than in the high-fat diet (Table 1), but cholesterol absorption can also be affected by body weight and serum cholesterol level itself [37,38]. We therefore assume that high-fat-diet–induced obesity and hypercholesterolemia markedly increased cholesterol absorption in mice fed a high-fat diet and that ezetimibe was more effective under such conditions.

In conclusion, the results of our study support the concept that ezetimibe may ameliorate hepatic insulin resistance as well as dyslipidemia and hepatic steatosis via a pathway involving SHP and SREBP-1c in high-fat-diet–induced obese mice.

Acknowledgment

We are grateful to the Schering-Plough Research Institute for providing us with the ezetimibe used in this study. We thank Mitsuyo Kaji and Eri Sakamoto for their excellent technical assistance and animal care. This work was supported by the Yokohama City University Center of Excellence Program of MEXT and a grant for the Strategic Research Project of Yokohama City University (to YT).

References

[1] Altmann SW, Davis HR, Zhu LJ, Yao X, Hoos LM, Tetzloff G, et al. Niemann-Pick C1 Like 1 protein is critical for intestinal cholesterol absorption. Science 2004;303:1201-4.

[2] Davies JP, Scott C, Oishi K, Liapis A, Ioannou YA. Inactivation of NPC1L1 causes multiple lipid transport defects and protects against diet-induced hypercholesterolemia. J Biol Chem 2005;280:12710-20.

[3] Valasek MA, Repa JJ, Quan G, Dietschy JM, Turley SD. Inhibiting intestinal NPC1L1 activity prevents diet-induced increase in biliary cholesterol in Golden Syrian hamsters. Am J Physiol Gastrointest Liver Physiol 2008;295:813-22.

[4] Deushi M, Nomura M, Kawakami A, Haraguchi M, Ito M, Okazaki M, et al. Ezetimibe improves liver steatosis and insulin resistance in obese rat model of metabolic syndrome. FEBS Lett 2007;581:5664-70.

[5] Labonté ED, Camarota LM, Rojas JC, Jandacek RJ, Gilham DE, Davies JP, et al. Reduced absorption of saturated fatty acids and resistance to diet-induced obesity and diabetes by ezetimibe-treated and Npc1l1−/− mice. Am J Physiol Gastrointest Liver Physiol 2008; 295:776-83.

[6] Assy N, Grozovski M, Bersudsky I, Szvalb S, Hussein O. Effect of insulin-sensitizing agents in combination with ezetimibe, and valsartan in rats with non-alcoholic fatty liver disease. World J Gastroenterol 2006;12:4369-76.

[7] Zheng S, Hoos L, Cook J, Tetzloff G, Davis Jr H, van Heek M, et al. Ezetimibe improves high fat and cholesterol diet-induced non-alcoholic fatty liver disease in mice. Eur J Pharmacol 2008;584: 118-24.

[8] Knopp RH, Dujovne CA, Beaut AL, Lipka LJ, Suresh R, Veltri EP. Evaluation of the efficacy, safety, and tolerability of ezetimibe in primary hypercholesterolaemia: a pooled analysis from two controlled phase III clinical studies. Int J Clin Pract 2003;57:363-8.

[9] Browning JD, Horton JD. Molecular mediators of hepatic steatosis and liver injury. J Clin Invest 2004;114:147-52.

[10] González-Ortiz M, Martínez-Abundis E, Kam-Ramos AM, Hernández-Salazar E, Ramos-Zavala MG. Effect of ezetimibe on insulin sensitivity and lipid profile in obese and dyslipidaemic patients. Cardiovasc Drug Ther 2006;20:143-6.

[11] Davis Jr HR, Compton DS, Hoos L, Tetzloff G. Ezetimibe, a potent cholesterol absorption inhibitor, inhibits the development of atherosclerosis in ApoE knockout mice. Arterioscler Thromb Vasc Biol 2001;21:2032-8.

[12] Folch J, Lees M, Sloane Stanley GH. A simple method for the isolation and purification of total lipids from animal tissues. J Biol Chem 1957;226:497.

[13] Usui S, Hara Y, Hosaki S, Okazaki M. A new on-line dual enzymatic method for simultaneous quantification of cholesterol and triglycerides in lipoproteins by HPLC. J Lipid Res 2002;43:805-14.

[14] Udagawa H, Kitaoka C, Sakamoto T, Kobayashi-Hattori K, Oishi Y, Arai S, et al. Serum cholesterol–decreasing effect of heat-moisture–treated high-amylose cornstarch in cholesterol-loaded rats. Biosci Biotechnol Biochem 2008;72:880-4.

[15] Terauchi Y, Takamoto I, Kubota N, Matsui J, Suzuki R, Komeda K, et al. Glucokinase and IRS-2 are required for compensatory beta cell hyperplasia in response to high-fat diet–induced insulin resistance. J Clin Invest 2007;117:246-57.

[16] Aoki K, Matsui J, Kubota N, Nakajima H, Iwamoto K, Takamoto I, et al. The role of the liver in glucose homeostasis in PI 3-kinase p85α deficient mice. Am J Physiol Endocrinol Metab 2009;296:E842-53.

[17] Kubota N, Terauchi Y, Kubota T, Kumagai H, Itoh S, Satoh H, et al. Pioglitazone ameliorates insulin resistance and diabetes by both adiponectin-dependent and -independent pathways. J Biol Chem 2006;281:8748-55.

[18] Suzuki R, Tobe K, Aoyama M, Inoue A, Sakamoto K, Yamauchi T, et al. Both insulin signaling defects in the liver and obesity contribute to insulin resistance and cause diabetes in Irs2(−/−) mice. J Biol Chem 2004;279:25039-49.

[19] Kubota N, Terauchi Y, Tobe K, Yano W, Suzuki R, Ueki K, Takamoto I, et al. Insulin receptor substrate 2 plays a crucial role in beta cells and the hypothalamus. J Clin Invest 2004;114:917-27.

[20] Berry MN, Friend DS. High-yield preparation of isolated rat liver parenchymal cells: a biochemical and fine structural study. J Cell Biol 1969;43:506-20.

[21] Seglen PO. Incorporation of radioactive amino acids into protein in isolated rat hepatocytes. Biochim Biophys Acta 1976;442:391-404.

[22] Shiroyama K, Moriwaki K, Yuge O. The direct effect of dopamine on glucose release from primary cultured rat hepatocytes. In Vivo 1998;12:527-9.

[23] Zhang G, Budker V, Wolff JA. High levels of foreign gene expression in hepatocytes after tail vein injections of naked plasmid DNA. Hum Gene Ther 1999;10:1735-7.

[24] Bisbis S, Bailbe D, Tormo MA, Picarel-Blanchot F, Derouet M, Simon J, et al. Insulin resistance in the GK rat: decreased receptor number but normal kinase activity in liver. Am J Physiol 1993;265:807-13.

[25] Song E, Lee SK, Wang J, Ince N, Ouyang N, Min J, et al. RNA interference targeting Fas protects mice from fulminant hepatitis. Nat Med 2003;9:226-7.

[26] McCaffrey AP, Meuse L, Pham TT, Conklin DS, Hannon GJ, Kay MA. RNA interference in adult mice. Nature 2002;418:38-9.

[27] Lewis DL, Hagstrom JE, Loomis AG, Wolff JA, Herweijer H. Efficient delivery of siRNA for inhibition of gene expression in postnatal mice. Nat Genet 2002;32:107-8.
[28] Watanabe M, Houten SM, Wang L, Moschetta A, Mangelsdorf DJ, Heyman RA, et al. Bile acids lower triglyceride levels via a pathway involving FXR, SHP, and SREBP-1c. J Clin Invest 2004;113: 1408-18.
[29] Ide T, Shimano H, Yahagi N, Matsuzaka T, Nakakuki M, Yamamoto T, et al. SREBPs suppress IRS-2–mediated insulin signalling in the liver. Nat Cell Biol 2004;6:351-7.
[30] Yamagata K, Daitoku H, Shimamoto Y, Matsuzaki H, Hirota K, Ishida J, et al. Bile acids regulate gluconeogenic gene expression via small heterodimer partner-mediated repression of hepatocyte nuclear factor 4 and Foxo1. J Biol Chem 2004;279:23158-65.
[31] Kamei Y, Miura S, Suganami T, Akaike F, Kanai S, et al. Regulation of SREBP1c gene expression in skeletal muscle: role of retinoid X receptor/liver X receptor and forkhead-O1 transcription factor. Endocrinology 2008;149:2293-305.
[32] Goodwin B, Jones SA, Price RR, Watson MA, McKee DD, Moore LB, et al. A regulatory cascade of the nuclear receptors FXR, SHP-1, and LRH-1 represses bile acid biosynthesis. Mol Cell 2000; 6:517-26.
[33] Lu TT, Makishima M, Repa JJ, Schoonjans K, Kerr TA, Auwerx J, et al. Molecular basis for feedback regulation of bile acid synthesis by nuclear receptors. Mol Cell 2000;6:507-15.
[34] Russell DW, Setchell KD. Bile acid biosynthesis. Biochemistry 1992;31:4737-49.
[35] Repa JJ, Turley SD, Quan G, Dietschy JM. Delineation of molecular changes in intrahepatic cholesterol metabolism resulting from diminished cholesterol absorption. J Lipid Res 2005;46:779-89.
[36] Mathur A, Walker JJ, Al-Azzawi HH, Lu D, Swartz-Basile DA, Nakeeb A, et al. Ezetimibe ameliorates cholecystosteatosis. Surgery 2007;142:228-33.
[37] Mok HY, von Bergmann K, Grundy SM. Effects of continuous and intermittent feeding on biliary lipid outputs in man: application for measurements of intestinal absorption of cholesterol and bile acids. J Lipid Res 1979;20:389-98.
[38] Kesäniemi YA, Miettinen TA. Cholesterol absorption efficiency regulates plasma cholesterol level in the Finnish population. Eur J Clin Invest 1987;17:391-5.

Blockade of class IB phosphoinositide-3 kinase ameliorates obesity-induced inflammation and insulin resistance

Naoki Kobayashi[a], Kohjiro Ueki[a,b,1], Yukiko Okazaki[a], Aya Iwane[a], Naoto Kubota[a,b,c], Mitsuru Ohsugi[a], Motoharu Awazawa[a,c], Masatoshi Kobayashi[a], Takayoshi Sasako[a], Kazuma Kaneko[a], Miho Suzuki[a], Yoshitaka Nishikawa[a], Kazuo Hara[a], Kotaro Yoshimura[d], Isao Koshima[d], Susumu Goyama[e], Koji Murakami[f], Junko Sasaki[g], Ryozo Nagai[h], Mineo Kurokawa[e], Takehiko Sasaki[g], and Takashi Kadowaki[a,b,c,1]

[a]Department of Metabolic Diseases, [d]Department of Plastic Surgery, [e]Department of Hematology and Oncology, and [h]Department of Cardiovascular Medicine, Graduate School of Medicine, and [b]Translational Systems Biology and Medicine Initiative (TSBMI), University of Tokyo, Tokyo 113-0033, Japan; [c]Division of Applied Nutrition, National Institute of Health and Nutrition, Tokyo 162-8636, Japan; [f]Discovery Research Laboratories, Kyorin Pharmaceutical Co., Ltd., Tochigi 329-0114, Japan; and [g]Division of Microbiology, Department of Pathology and Immunology, Akita University School of Medicine, Akita 010-8543, Japan

Edited* by Lewis Clayton Cantley, Beth Israel Deaconess Medical Center, Boston, MA, and approved February 23, 2011 (received for review November 2, 2010)

Obesity and insulin resistance, the key features of metabolic syndrome, are closely associated with a state of chronic, low-grade inflammation characterized by abnormal macrophage infiltration into adipose tissues. Although it has been reported that chemokines promote leukocyte migration by activating class IB phosphoinositide-3 kinase (PI3Kγ) in inflammatory states, little is known about the role of PI3Kγ in obesity-induced macrophage infiltration into tissues, systemic inflammation, and the development of insulin resistance. In the present study, we used murine models of both diet-induced and genetically induced obesity to examine the role of PI3Kγ in the accumulation of tissue macrophages and the development of obesity-induced insulin resistance. Mice lacking p110γ (*Pik3cg*$^{-/-}$), the catalytic subunit of PI3Kγ, exhibited improved systemic insulin sensitivity with enhanced insulin signaling in the tissues of obese animals. In adipose tissues and livers of obese *Pik3cg*$^{-/-}$ mice, the numbers of infiltrated proinflammatory macrophages were markedly reduced, leading to suppression of inflammatory reactions in these tissues. Furthermore, bone marrow-specific deletion and pharmacological blockade of PI3Kγ also ameliorated obesity-induced macrophage infiltration and insulin resistance. These data suggest that PI3Kγ plays a crucial role in the development of both obesity-induced inflammation and systemic insulin resistance and that PI3Kγ can be a therapeutic target for type 2 diabetes.

Type 2 diabetes and metabolic syndrome, the major risk factors of cardiovascular disease and related death, are explosively increasing worldwide due to a pandemic of obesity that induces a variety of disorders, such as insulin resistance and hepatic steatosis (1, 2). Recent studies have revealed that obesity induces hematopoietic cell infiltration into adipose tissue, which in turn enhances adipose tissue inflammation and the secretion of proinflammatory adipokines, leading to systemic insulin resistance (3–8). Inhibition of macrophage infiltration into adipose tissue could be considered a therapeutic strategy on the basis of the accumulated evidence of obesity-related metabolic disorders.

It has been known that chemokines initiate chemotaxis by binding the corresponding G protein-coupled receptors (GPCRs), leading to activation of class IB phosphoinositide-3 kinase (PI3Kγ) (9). Upon chemokine stimulation, the unidirectional cytoskeletal rearrangement caused by PI3Kγ promotes cell movement toward the higher concentration of the chemokine. Furthermore, previous studies using mice lacking p110γ (*Pik3cg*$^{-/-}$ mice), the catalytic subunit of the PI3Kγ complex, demonstrated that PI3Kγ is essential for chemotaxis in leukocytes, including macrophages (10, 11). However, the role of PI3Kγ in obesity-induced macrophage infiltration into tissues, systemic inflammation, and the development of insulin resistance is still unknown.

To investigate the role of PI3Kγ in obesity-induced insulin resistance, we analyzed *Pik3cg*$^{-/-}$ mice fed a high-fat diet (HFD) and those with a genetically obese diabetic background and found that these mice exhibit improved insulin sensitivity along with decreased macrophage infiltration and inflammatory changes. Moreover, we have also demonstrated that a pharmacological inhibitor of PI3Kγ ameliorates obesity-induced diabetes.

Results

Mice Lacking PI3Kγ Were Protected from HFD-Induced Insulin Resistance. We fed *Pik3cg*$^{-/-}$ and wild-type control (*Pik3cg*$^{+/+}$) mice a normal diet (ND) or a HFD. While receiving ND, *Pik3cg*$^{-/-}$ mice grew normally and showed no significant differences in glucose metabolism, insulin sensitivity, and glucose tolerance compared with *Pik3cg*$^{+/+}$ mice (Fig. S1). These data suggest that PI3Kγ is not required for normal growth nor for maintenance of glucose homeostasis during ND conditions. In contrast, HFD-fed *Pik3cg*$^{-/-}$ mice maintained significantly lower blood glucose and insulin levels under random-fed conditions and also showed better response to insulin as estimated by an insulin tolerance test (ITT) (Fig. 1 *A–C*), indicating that lack of PI3Kγ led to protection from HFD-induced insulin resistance. Reflecting the improved systemic insulin sensitivity, insulin concentrations of *Pik3cg*$^{-/-}$ mice were significantly lower than those of *Pik3cg*$^{+/+}$ mice during the glucose tolerance test (GTT) whereas both groups of mice showed similar blood glucose levels (Fig. 1*D*). Furthermore, we observed significantly enhanced insulin signaling in liver and muscle of HFD-fed *Pik3cg*$^{-/-}$ mice (Fig. 1 *E* and *F* and Fig. S2). To investigate the impact of the lower weight gain of *Pik3cg*$^{-/-}$ mice compared with *Pik3cg*$^{+/+}$ mice under HFD-fed conditions without any differences in food intake and energy expenditure (Table S1), we fed *Pik3cg*$^{+/+}$ mice a limited HFD to match the weight gain of *Pik3cg*$^{-/-}$ mice. *Pik3cg*$^{-/-}$ mice still displayed better insulin sensitivity even compared with the weight-matched *Pik3cg*$^{+/+}$ mice (Fig. S3). These results suggest that PI3Kγ is required for HFD-induced systemic insulin resistance and that the body weight change does not seem to be a major cause of improved insulin sensitivity observed in HFD-fed *Pik3cg*$^{-/-}$ mice.

Author contributions: N. Kobayashi, K.U., and T.K. designed research; N. Kobayashi, K.U., Y.O., A.I., N. Kubota, M.O., M.A., M. Kobayashi, T. Sasako, K.K., M.S., Y.N., and S.G. performed research; K.Y., I.K., K.M., J.S., and T. Sasaki contributed new reagents/analytic tools; N. Kobayashi, K.U., K.H., R.N., and M. Kurokawa analyzed data; and N. Kobayashi, K.U., and T.K. wrote the paper.

The authors declare no conflict of interest.

*This Direct Submission article had a prearranged editor.

[1]To whom correspondence may be addressed. E-mail: ueki-tky@umin.ac.jp or kadowaki-3im@h.u-tokyo.ac.jp.

This article contains supporting information online at www.pnas.org/lookup/suppl/doi:10.1073/pnas.1016430108/-/DCSupplemental.

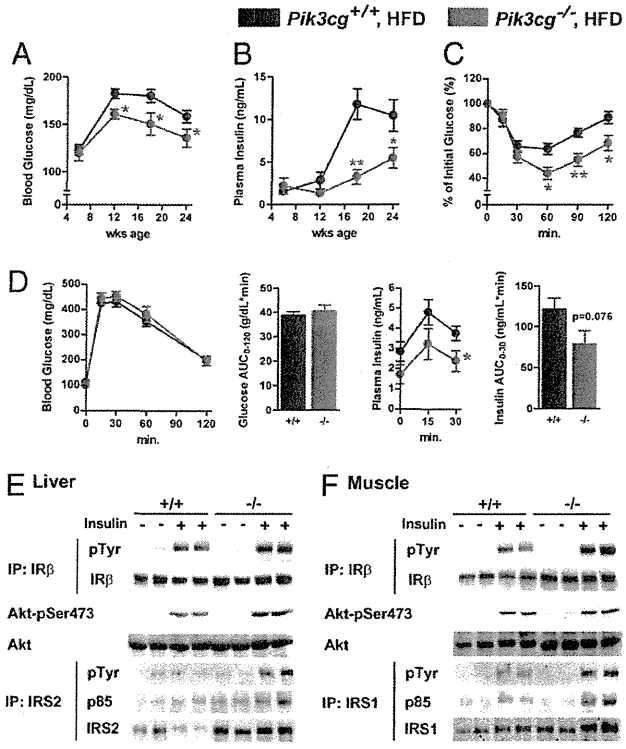

Fig. 1. Mice lacking PI3Kγ were protected from HFD-induced insulin resistance. (*A* and *B*) Blood glucose (*A*) and plasma insulin levels (*B*) in *Pik3cg*$^{+/+}$ and *Pik3cg*$^{-/-}$ mice fed on a HFD from 6 to 24 wk of age (n = 15–20). (*C*) Glucose levels during ITT (23 wk of age) were determined at the indicated time points after i.p. injection with a bolus of insulin [1.0 U·kg^{-1} body weight (BW)] (n = 7–8). (*D*) Glucose and insulin levels during GTT (24 wk of age) were determined at the indicated time points after i.p. injection with a bolus of glucose (1.5 g·kg^{-1} BW) (n = 7–8). (*E* and *F*) Phosphorylation of insulin receptor β-subunit (IRβ), insulin receptor substrate (IRS-1, IRS-2), and Akt induced by a bolus injection of insulin was assessed in livers (*E*) and skeletal muscles (*F*) of *Pik3cg*$^{+/+}$ ($^{+/+}$) and *Pik3cg*$^{-/-}$ ($^{-/-}$) mice fed a HFD (n = 3–4). IP, immunoprecipitated; pTyr, phosphorylated tyrosine; pSer, phosphorylated serine. *P < 0.05, **P < 0.01.

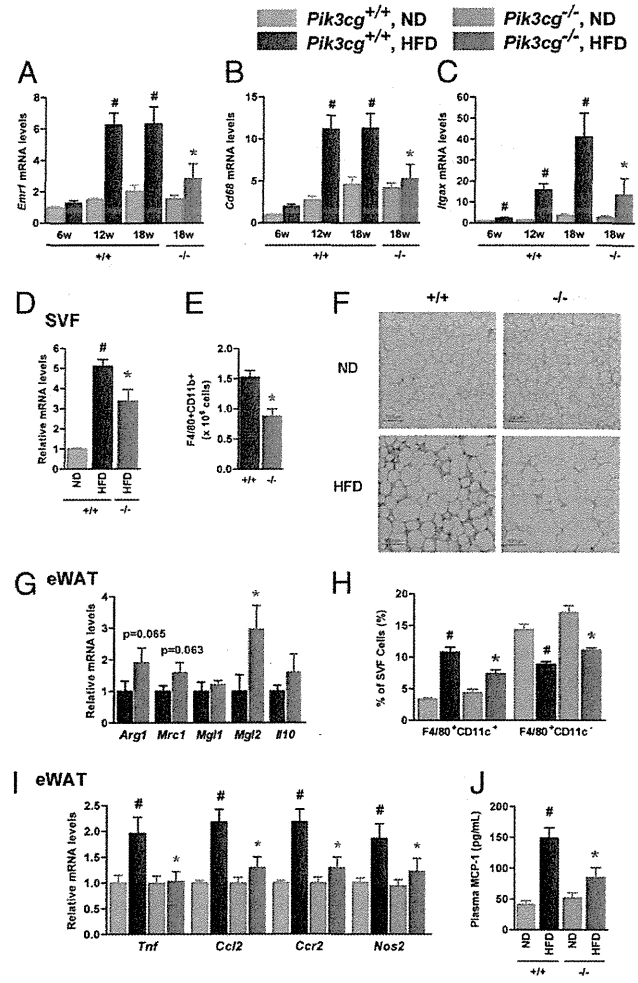

Fig. 2. Loss of PI3Kγ decreased macrophage infiltration into adipose tissue and markedly suppressed proinflammatory changes induced by a HFD. (*A–C*) Expression levels of *Emr1* (F4/80, *A*), *Cd68* (*B*), and *Itgax* (CD11c, *C*) in eWAT of *Pik3cg*$^{+/+}$ ($^{+/+}$) and *Pik3cg*$^{-/-}$ ($^{-/-}$) mice fed a ND or a HFD for the indicated periods (n = 6–8). (*D* and *E*) Expression levels of *Cd68* (*D*) and the population of macrophages (F4/80$^+$CD11b$^+$) measured by FACS analysis (*E*) in SVF from the eWAT (n = 4–5). (*F*) Immunohistochemical analysis of adipose tissue macrophages. eWAT of mice fed ND or HFD were stained with antibody against F4/80. (Scale bar, 100 μm.) (*G*) Expression levels of M2 macrophage-specific genes in eWAT of *Pik3cg*$^{+/+}$ and *Pik3cg*$^{-/-}$ mice fed on a HFD (normalized to *Cd68*) (n = 6–8). (*H*) Quantification of M1 macrophage (F4/80$^+$CD11c$^+$) and M2 macrophage (F4/80$^+$CD11c$^-$) in SVF from eWAT of mice fed on a ND or a HFD (n = 5). (*I*) Expression levels of proinflammatory genes in eWAT (n = 6–8). (*J*) Serum levels of MCP-1 in *Pik3cg*$^{+/+}$ and *Pik3cg*$^{-/-}$ mice fed on a ND or a HFD (n = 6–8). #P < 0.05 for HFD compared with ND. *P < 0.05 for *Pik3cg*$^{-/-}$ mice compared with *Pik3cg*$^{+/+}$ controls.

Loss of PI3Kγ Markedly Decreased the Number of Infiltrated Macrophages and the Amount of Inflammation in Adipose Tissue Induced by HFD. To clarify the mechanisms leading to the improvement of HFD-induced insulin resistance, we investigated the infiltrated macrophage contents in the epididymal adipose tissue (eWAT) of *Pik3cg*$^{-/-}$ and *Pik3cg*$^{+/+}$ mice. HFD feeding progressively increased the expression of macrophage-specific markers in the eWAT of *Pik3cg*$^{+/+}$ mice (Fig. 2 *A* and *B*). By contrast, the levels of macrophage-specific markers were markedly decreased in the eWAT, particularly in the stromal vascular fraction of *Pik3cg*$^{-/-}$ mice under HFD-fed conditions (Fig. 2 *A*, *B*, and *D*), although no significant differences in adiposity, adipocyte size, and the expression levels of genes involved in adipocyte function were observed between *Pik3cg*$^{+/+}$ and *Pik3cg*$^{-/-}$mice (Fig. S4*A* and Table S1). Fluorescence-activated cell sorting (FACS) and histological analyses also showed significant reductions of adipose tissue macrophages (ATMs) in HFD-fed *Pik3cg*$^{-/-}$ mice (Fig. 2 *E* and *F*). Expression of *Itgax* (coding CD11c), which has been reported to increase in the eWAT of mice fed a HFD (12, 13), was markedly suppressed in *Pik3cg*$^{-/-}$ mice (Fig. 2*C*). By contrast, the relative levels of genes preferentially expressed in M2 macrophages (14) were increased in the eWAT of *Pik3cg*$^{-/-}$ mice (Fig. 2*G*). FACS analysis also revealed that HFD feeding in *Pik3cg*$^{+/+}$ mice decreased the F4/80$^+$CD11c$^-$ population in the stromal vascular cells of eWAT accompanied by a 3.2-fold increase in the F4/80$^+$CD11c$^+$ population (Fig. 2*H*). Conversely, *Pik3cg* deletion significantly decreased the HFD-induced F4/80$^+$CD11c$^+$ double-positive cells enrichment but not that of F4/80$^+$CD11c$^-$ in the eWAT of HFD-fed mice (Fig. 2*H*). These changes resulted in a shift-up in the ratio of M2 to M1 macrophages in *Pik3cg*$^{-/-}$ HFD-fed mice. Because CD8$^+$ T cells have recently been reported to contribute to obesity-induced inflammation in adipose tissue and systemic insulin resistance (15), we assessed the *Cd8* expression level in the eWAT of HFD-fed mice and found a small and nonsignificant reduction in the eWAT of *Pik3cg*$^{-/-}$ mice (Fig. S4*C*), suggesting that deletion of PI3Kγ more prominently affected the infiltration of M1 macrophages. To gain additional insight into the clinical importance of PI3Kγ in the fat of obese subjects, we analyzed the expression of *PIK3CG* in s.c. adipose

tissue samples of humans with a wide range of values for body mass index (BMI) (16.4–32.0). Levels of *PIK3CG* expression showed a strong correlation with BMI ($P = 0.0009$) and also correlated with *ITGAX* expression levels ($P = 0.0087$) (Fig. S5).

ATMs have been identified as the major source of inflammatory cytokine/adipokine production in the adipose tissues of obese subjects, and these chemokines are thought to be a cause of chronic inflammation and systemic insulin resistance in obesity (3). Consistent with this idea, expression levels of *Tnf*, *Ccl2*, *Ccr2*, and *Nos2* in the eWAT of HFD-fed mice were increased, whereas these increases were significantly attenuated by PI3Kγ deletion (Fig. 2*I*). Furthermore, circulating monocyte chemotactic protein-1 (MCP-1) levels also decreased with a trend toward reductions in c-jun N-terminal kinase, and IκB kinase phosphorylation in the eWAT of *Pik3cg*$^{-/-}$ mice (Fig. 2*J* and Fig. S4 *E* and *F*). Taken together, these data suggest that the loss of PI3Kγ specifically suppresses M1 macrophage infiltration, leading to suppression of HFD-induced inflammation in adipose tissue, and finally leading to improved insulin sensitivity.

However, it remained possible that deficiency of PI3Kγ would modulate insulin sensitivity through other mechanisms. Indeed, we found that elevated leptin levels observed during HFD feeding were significantly decreased with a trend to decrease *Socs3* expression by deletion of PI3Kγ (Fig. S4 *G* and *H*), suggesting improved leptin sensitivity. This could be caused by reductions of proinflammatory adipokines and also through reduced macrophage infiltration in the hypothalamus by deletion of PI3Kγ, as evidenced by deceased expression of *Emr1* (Fig. S4*H*). However, the effect appeared very limited because food intake, energy expenditure, and genes regulated by leptin were not altered by deletion of PI3Kγ.

Loss of PI3Kγ Ameliorated Diet-Induced Hepatic Steatosis. Next, we assessed the impact of PI3Kγ deficiency on HFD-induced hepatic steatosis, which is known to be tightly associated with hepatic and systemic insulin resistance (16, 17). Interestingly, hepatic triglyceride content was significantly suppressed in the livers of *Pik3cg*$^{-/-}$ mice compared with that seen in *Pik3cg*$^{+/+}$ mice, which is consistent with the histological findings by hematoxylin and eosin (H&E) staining (Fig. 3*A* and *B*). Hepatic steatosis can be caused by overproduction of fatty acid, reduced fatty acid oxidation, increased lipid transport, and their combinations. Expression levels of genes involved in fatty acid synthesis tested here were not affected by PI3Kγ deletion (Fig. 3*C*, *Upper*), whereas *Cpt1a*, which involves fatty acid oxidation, was significantly increased in HFD-fed *Pik3cg*$^{-/-}$ mice compared with *Pik3cg*$^{+/+}$ mice (Fig. 3*C*, *Upper*). Intriguingly, expression of *Cidec* (encoding Fsp27) and *Cd36* in HFD-fed conditions was markedly suppressed in the livers of *Pik3cg*$^{-/-}$ mice (Fig. 3*C*, *Lower*). Expression of peroxisome proliferator-activated receptors (PPARγ), which is known to directly regulate *Cidec*, *Cd36*, *Scd1*, and *Pparg* itself (18–22), was also significantly decreased by deletion of PI3Kγ (Fig. 3*C*, *Lower*). Moreover, similar to findings seen with eWAT, expression of *Cd68*, *Tnf*, *Ccl2*, and its receptor *Ccr2* was significantly decreased in the livers of *Pik3cg*$^{-/-}$ mice compared with that seen in *Pik3cg*$^{+/+}$ mice (Fig. 3 *D* and *E*), and M2 macrophage markers (*Arg1*, *Mrc1*, *Mgl1*, and *Mgl2*) were up-regulated (Fig. 3*F*). The MCP-1/chemokine (C-C motif) receptor 2 (CCR2) pathway, which lies upstream of PI3Kγ, has been reported to contribute to the development of hepatic steatosis (6, 23, 24), and our findings may provide a missing link between hepatic steatosis and inflammation.

Loss of PI3Kγ in *ob/ob* Mice Reduced Inflammatory Changes in Adipose Tissue, Leading to Improvement of Insulin Sensitivity. To further assess the role of PI3Kγ in obesity-induced inflammation and insulin resistance, we generated *Pik3cg*$^{-/-}$ mice with a leptin-deficient background (*Pik3cg*$^{-/-}$*:ob/ob*). Although *Pik3cg*$^{-/-}$*:ob/ob* mice gained body weight in a similar manner compared with *Pik3cg*$^{+/+}$*:ob/ob* mice, they displayed lower blood glucose levels up to 20 wk of age (Fig.4 *A* and *B*). Similarly, *Pik3cg*$^{-/-}$*:ob/ob* mice also displayed significantly decreased glucose levels in a fasted state as well as during ITT and GTT (Fig. 4 *C* and *D*) along with enhanced insulin-stimulated Akt (also known as protein kinase B or PKB) phosphorylation in both liver and muscle

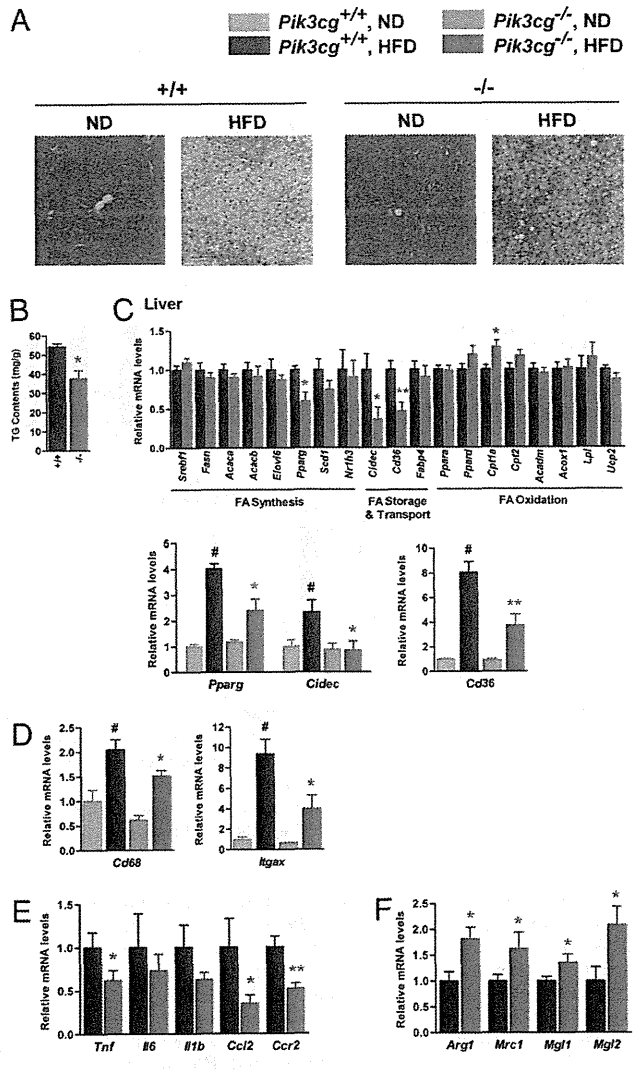

Fig. 3. PI3Kγ knockout mice showed amelioration of HFD-induced hepatic steatosis. (*A*) Hematoxylin and eosin-stained sections of liver from *Pik3cg*$^{+/+}$ ($^{+/+}$) and *Pik3cg*$^{-/-}$ ($^{-/-}$) mice on a ND or a HFD. (Scale bar, 100 μm.) (*B*) Triglyceride (TG) content in liver of mice on a HFD ($n = 7$–8). (*C*) Expression levels of mRNA related to fatty acid metabolism in liver of fasted mice ($n = 7$–8). (*D*–*F*) Expression levels of genes encoded macrophage-related protein (*D*), proinflammatory genes (*E*), and M2 macrophage-specific genes (normalized to *Cd68*, *F*) in liver ($n = 7$–8). #$P < 0.05$ for a HFD compared with ND. *$P < 0.05$ and **$P < 0.01$ for *Pik3cg*$^{-/-}$ mice compared with *Pik3cg*$^{+/+}$ controls.

of *Pik3cg*$^{-/-}$*:ob/ob* mice (Fig. 4*E*). In addition, the expression of *Emr1*, *Cd68*, and *Tnf* in the eWAT of *Pik3cg*$^{-/-}$*:ob/ob* mice was also significantly decreased (Fig. 4 *F* and *G*), whereas M2 macrophage markers were up-regulated (Fig. 4*H*). These data suggest that loss of PI3Kγ ameliorated obesity-induced insulin resistance through the reduction of macrophage infiltration and inflammation even in a genetically obese model and that a large part of these beneficial effects of PI3Kγ deficiency on glucose metabolism appears to be independent of leptin signaling and body weight change.

Bone Marrow-Specific Deletion of PI3Kγ Ameliorates Obesity-Induced Diabetes. Although PI3Kγ is almost exclusively expressed in hematopoietic cells, to rule out the possibility that PI3Kγ in extrahematopoietic parenchymal tissues might play some role in glucose metabolism, we generated a bone marrow (BM)-specific PI3Kγ deletion in *ob/ob* [*Pik3cg*$^{-/-}$ bone marrow transplant

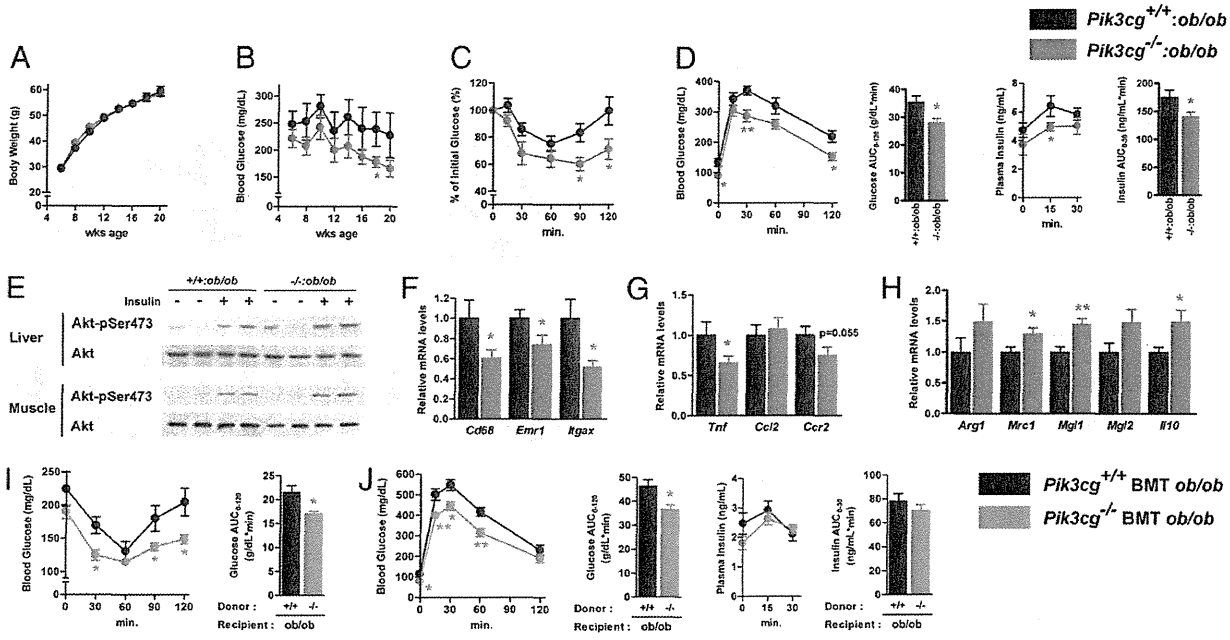

Fig. 4. Loss of PI3Kγ in the *ob/ob* background improved insulin sensitivity. (*A* and *B*) Time course of body weight (*A*) and blood glucose (*B*) in *Pik3cg*$^{+/+}$*:ob/ob* and double-mutant *Pik3cg*$^{-/-}$*:ob/ob* mice (n = 12–18). (*C*) Glucose levels during ITT (8 wk of age) were determined at the indicated time points after i.p. injection with a bolus of insulin (2.0 U·kg^{-1} BW) (n = 7–8). (*D*) Glucose and insulin levels during GTT (9 wk of age) were determined at the indicated time points after i.p. injection with a bolus of glucose (1.0 g·kg^{-1} BW) (n = 7–8). (*E*) Phosphorylation of Akt in livers and skeletal muscles induced by a bolus injection of insulin was assessed. (*F–H*) Expression levels of genes encoded macrophage-related protein (*F*), proinflammatory genes (*G*), and M2 macrophage-specific genes (normalized to *Cd68*, *H*) in eWAT (n = 7–8). (*I* and *J*) Bone marrow-specific PI3Kγ knockout *ob/ob* mice were generated by bone marrow transplantation. (*I*) Glucose levels during ITT were determined at the indicated time points after i.p. injection with a bolus of insulin (2.0 U·kg^{-1} BW). (*J*) Glucose and insulin levels during GTT were determined at the indicated time points after i.p. injection with a bolus of glucose (1.0 g·kg^{-1} BW) (n = 6). *$P < 0.05$, **$P < 0.01$.

(BMT) *ob/ob*] mice by BM transplantation. Compared with the control mice that received the *Pik3cg*$^{+/+}$ BM cells, *Pik3cg*$^{-/-}$ BMT *ob/ob* mice displayed improved glucose levels, systemic insulin sensitivity, and glucose intolerance (Fig. 4 *I* and *J*), as observed in *ob/ob* mice systemically lacking *Pik3cg*$^{-/-}$. These data strongly suggest that the metabolic phenotypes of *Pik3cg*$^{-/-}$*:ob/ob* mice are mainly owing to the lack of PI3Kγ in BM-derived cells. Moreover, we also confirmed that BM-specific *Pik3cg*$^{-/-}$ (*Pik3cg*$^{-/-}$ BMT) mice fed a HFD exhibited the phenotypes similar to those of mice systemically lacking *Pik3cg*$^{-/-}$ (Fig. S6). Furthermore, the in vitro studies revealed that lack of PI3Kγ did not significantly alter expression of *Itgax* in BM-derived macrophages (BMDM), induction of *Mgl2* in IL-4–stimulated alternative activation in BMDM, or LPS-stimulated proinflammatory cytokine expression in peritoneal macrophages (Fig. S7 *A–C*).

Blockade of PI3Kγ by a Pharmacological Inhibitor Ameliorated Obesity-Induced Diabetes. Finally, we addressed whether pharmacological inhibition of PI3Kγ could ameliorate insulin resistance in obese diabetic animal models using AS-605240, a small-molecule inhibitor for PI3Kγ (25). We confirmed that AS-605240 selectively blocked class IB PI3K signaling in cultured macrophages (Fig. S7*D*), as shown in the previous reports (26, 27). Treatment with 10 mg/kg/d of AS-605240 lowered blood glucose levels, with an associated significant improvement of both insulin sensitivity and glucose tolerance (Fig. 5 *A–C*) without affecting body weight (54.2 ± 0.8 g for vehicle, 54.0 ± 0.5 g for 10 mg/kg/d of AS-605240). A total of 30 mg/kg/d of AS-605240 displayed more profound effects (Fig. 5 *A–C*) with slightly less weight gain (49.5 ± 0.8 g). Moreover, AS-605240 dose-dependently reduced the abundance of ATMs as estimated by F4/80 staining and the expression levels of macrophage markers in eWAT (Fig. 5 *D* and *E*). As a consequence, the circulating levels of MCP-1 were also reduced in *ob/ob* mice treated with AS-605240 (Fig. 5*F*). We also confirmed that *Pik3cg*$^{+/+}$ mice fed a HFD treated with AS-605240 exhibited metabolic phenotypes very similar to those of *Pik3cg*$^{-/-}$ mice (Fig. S8). These findings strongly suggest that pharmacological intervention by inhibiting PI3Kγ is effective even after establishment of a morbidly obese condition.

Discussion

Obesity causes a variety of metabolic disorders, including diabetes and fatty liver disease, initiated by macrophage infiltration into adipose tissue and presumably also into liver. Previous studies have shown that MCP-1 triggers this macrophage infiltration and that modulation of the MCP-1/CCR2 signaling by genetic disruption or treatment with an inhibitory molecule can ameliorate obesity-induced insulin resistance (5, 6, 23, 24, 28). Other chemokines have recently been suggested to also promote macrophage infiltration in obesity (8, 29, 30). Receptors for these chemokines, including CCR2, are GPCRs, of which PI3Kγ lies downstream and mediates the signal to promote cell movement in response to chemokine stimulation (10, 11, 31, 32). Here, we show that suppression of PI3Kγ activity attenuates obesity-induced proinflammatory macrophage infiltration into adipose tissue and liver, leading to improvement of insulin resistance.

HFD feeding markedly increases CD11c-positive macrophages in eWAT as well as in the liver of *Pik3cg*$^{+/+}$ mice, whereas the increase is significantly suppressed by disruption of PI3Kγ. By contrast, the expression of the M2 macrophage marker is not decreased in these tissues of *Pik3cg*$^{-/-}$ mice fed a HFD, leading to an increase in the ratio of M2 to M1. This is because M1 macrophages, but not M2 macrophages, abundantly express CCR2 that promotes cell migration into both adipose tissue and liver via PI3Kγ activation. Furthermore, the results of BMT experiments using *ob/ob* or HFD-fed mice clearly demonstrate that the improved glucose metabolism caused by a lack of PI3Kγ is largely attributed to BM cells. Together with the results of in vitro experiments, the improved insulin sensitivity and glucose homeostasis associated with decreased inflammatory changes in the adipose tissue and liver of obese *Pik3cg*$^{-/-}$ mice

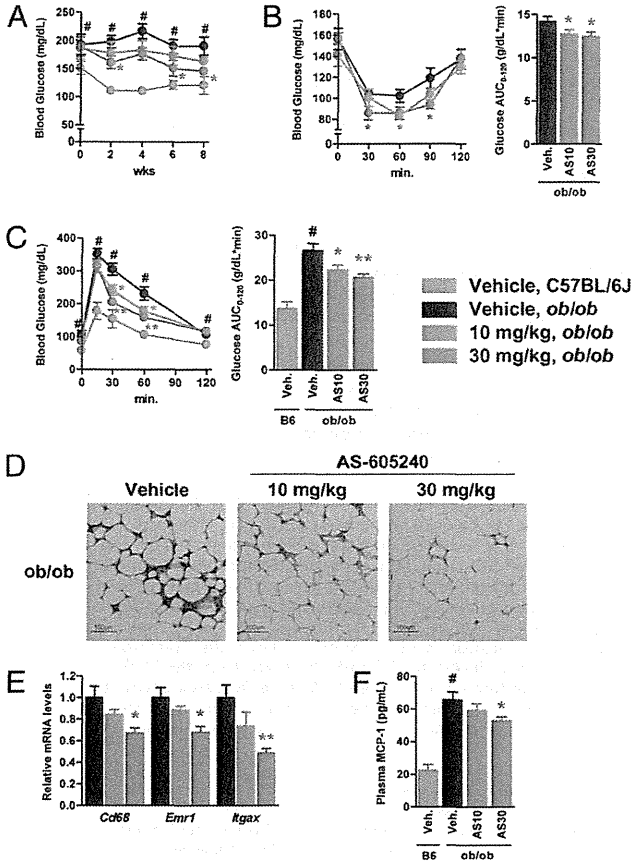

Fig. 5. Blockade of PI3Kγ by a pharmacological inhibitor ameliorated diabetes in *ob/ob* mice. *ob/ob* mice were treated with a PI3Kγ inhibitor, AS-605240, from 6 wk of age for 8 wk. Age-matched C57BL/6J mice served as lean controls. (*A*) Time course of blood glucose levels in vehicle, 10 or 30 mg/kg/d of AS-605240–treated *ob/ob* mice (designated as AS10 or AS30, respectively), and vehicle-treated C57BL/6J mice. (*B* and *C*) Glucose levels during ITT (7 wk treatment, *B*) or GTT (8 wk treatment, *C*) in vehicle (Veh.) or AS-605240–treated *ob/ob* mice were determined at the indicated time points after i.p. injection with a bolus of insulin (1.0 U·kg^{-1} BW) for ITT or glucose (1.5 g·kg^{-1} BW) for GTT. (*D*) Immunohistochemical analysis of adipose tissue macrophage. eWAT of *ob/ob* mice treated with vehicle or AS-605240 were stained with antibody against F4/80. (Scale bar, 100 μM.) (*E*) Expression levels of genes encoded macrophage-related protein in eWAT of vehicle or AS-605240–treated *ob/ob* mice. (*F*) Serum MCP-1 levels in vehicle or AS-605240–treated *ob/ob* mice and vehicle-treated C57BL/6J mice. (n = 7–8). #$P < 0.05$ for vehicle-treated *ob/ob* compared with vehicle-treated C57BL/6J mice. *$P <$ 0.05 and **$P < 0.01$ for AS-605240–treated *ob/ob* compared with vehicle-treated *ob/ob* control.

are largely due to a reduction in the number of infiltrated M1 macrophages that produce proinflammatory adipokines, which thereby promotes systemic insulin resistance, but not the functional changes or differentiation defects in these cells.

Hepatic steatosis is also known to exacerbate insulin resistance in obesity and cause liver dysfunction, such as nonalcoholic steatohepatitis (33). In the liver of *Pik3cg*$^{-/-}$ mice, expression of *Pparg* and *Cidec* is significantly decreased without any alterations in genes involved in fatty acid synthesis, whereas genes regulating β-oxidation, such as *Cpt1a*, are up-regulated, consistent with the previous report that Fsp27 suppresses β-oxidation and triglyceride turnover in hepatocytes (21). Fsp27 has been reported to regulate lipid droplet formation downstream of PPARγ in adipocytes, and deletion of Fsp27 leads to protection from diet-induced obesity (22), although it is unclear whether Fsp27 also functions as a key regulator of lipid droplet formation in hepatocytes. Meanwhile, PPARγ expression levels in the eWAT of *Pik3cg*$^{-/-}$ mice are not suppressed differently from those in liver. It is proposed that, when the capacity of lipid storage in adipose tissue, presumably regulated by PPARγ, reaches a limit, accumulation of lipids in extra-adipose tissue, such as liver and muscle, takes place, leading to insulin resistance (1, 16). Moreover, it has been suggested that suppression of inflammation reduces the development of hepatic steatosis and insulin resistance. Indeed, treatment with a CCR2 inhibitor ameliorates insulin resistance and hepatic steatosis in *db/db* mice associated with significant reductions in the expression of CD36 in liver (23). Although it remains unclear how PI3Kγ deficiency causes the suppression of lipid accumulation in liver, it is possible that inhibition of macrophage infiltration into adipose tissue and liver, and the subsequent reduction of inflammatory changes, can decrease PPARγ expression in liver but not in adipocytes. This may inhibit the ectopic lipid accumulation, leading to systemic insulin sensitivity, although it should be explored how PPARγ is regulated in these tissues.

Inhibitors for PI3Kδ and PI3Kγ are expected to be therapeutic agents for chronic inflammatory diseases (34, 35). Indeed, pharmacological inhibition of PI3Kγ ameliorates rheumatoid arthritis, lupus nephritis, and atherosclerosis in mouse models (25, 27, 34, 36), and here we provide evidence that the PI3Kγ inhibition is also promising for treatment of obesity-induced diabetes. Because multiple chemokine-signaling pathways can be involved in macrophage infiltration and inflammation in an obese context, and because inhibition of PI3Kγ could suppress macrophage migration caused by all these chemokines (8, 34), blockade of PI3Kγ appears to have advantages compared with the strategies to inhibit single chemokine signaling, such as MCP-1 or CCR2, which have been shown to improve insulin sensitivity in obese mice (6, 23, 28). However, a highly selective inhibitor for PI3Kγ, which does not affect class IA PI3Ks and other kinases, should be developed and carefully evaluated for clinical use to avoid potential adverse effects, such as inhibition of insulin signaling. Nevertheless, our data suggest that PI3Kγ inhibition can be a strategy for treating obesity-induced insulin resistance.

We have clearly demonstrated that PI3Kγ plays a crucial role in obesity-induced inflammation, hepatic steatosis, and systemic insulin resistance and that inhibition of PI3Kγ activity ameliorates obesity-induced insulin resistance, at least in part, due to the reductions in macrophage infiltration and subsequent inflammatory responses in both adipose tissue and liver. These findings provide a possibility for a therapeutic approach to obesity-induced diabetes and fatty liver disease.

Materials and Methods

Mice. We generated *Pik3cg*$^{-/-}$ mice as previously described (11) and used these mice after they were backcrossed to C57BL/6J mice for more than 16 generations with C57BL/6J mice as the controls. *Pik3cg*$^{-/-}$:*ob/ob* mice were generated by intercrossing *Pik3cg*$^{+/-}$:*ob/+* mice. All mice were housed under a 12-h light/12-h dark cycle and had free access to sterile water and pellet food ad libitum except when fed a limited HFD. The animal care and experimental procedures were approved by the Animal Care Committee of the University of Tokyo.

Metabolic Studies. Male *Pik3cg*$^{-/-}$ and *Pik3cg*$^{+/+}$ mice were fed a standard chow (CE-2; CLEA Japan) or high-fat/high-caloric diet (high fat diet 32; CLEA Japan). For ITTs, mice received i.p. injections of human insulin (Humalin R; Eli Lilly) in the ad libitum feeding state. For GTTs, mice received i.p. injections of glucose after an overnight fast. Blood glucose levels were measured using a Glutest sensor (Sanwa Chemical) at the indicated time points, and the plasma insulin levels were measured using a RIA kit (Biotrek), as previously described (37).

Insulin-Signaling Analysis. Mice were anesthetized after 16 h of fasting, and human insulin was injected into the inferior vena cava. After 5 min, tissues were quickly excised and frozen in liquid nitrogen. Tissue lysates were prepared and used for immunoprecipitation and immunoblotting as previously described (38).